NASA TECHNICAL NOTE

NASA TN D-6904

NASA TN D-6904

A FLIGHT EVALUATION OF METHODS FOR PREDICTING VORTEX WAKE EFFECTS ON TRAILING AIRCRAFT

by Glenn H. Robinson and Richard R. Larson

Flight Research Center
Edwards, Calif. 93523

NATIONAL AERONAUTICS AND SPACE ADMINISTRATION • WASHINGTON, D. C. • NOVEMBER 1972

1. Report No. NASA TN D-6904	2. Government Accession No.	3. Recipient's Catalog No.
4. Title and Subtitle A FLIGHT EVALUATION OF METHODS FOR PREDICTING VORTEX WAKE EFFECTS ON TRAILING AIRCRAFT		5. Report Date November 1972 6. Performing Organization Code
7. Author(s) Glenn H. Robinson and Richard R. Larson		8. Performing Organization Report No. H-712 10. Work Unit No. 760-67-04-00-24
9. Performing Organization Name and Address NASA Flight Research Center P. O. Box 273 Edwards, California 93523		11. Contract or Grant No. 13. Type of Report and Period Covered Technical Note
12. Sponsoring Agency Name and Address National Aeronautics and Space Administration Washington, D. C. 20546		14. Sponsoring Agency Code

15. Supplementary Notes

16. Abstract

The results of four current analytical methods for predicting wing vortex strength and decay rate are compared with the results of a flight investigation of the wake characteristics of several large jet transport aircraft. An empirical expression defining the strength and decay rate of wake vortices is developed that best represents most of the flight-test data. However, the expression is not applicable to small aircraft that would be immersed in the vortex wake of large aircraft.

17. Key Words (Suggested by Author(s))	18. Distribution Statement
Wingtip vortex models Vortex wake effects	Unclassified - Unlimited

19. Security Classif. (of this report)	20. Security Classif. (of this page)	21. No. of Pages	22. Price*
Unclassified	Unclassified	58	$3.00

* For sale by the National Technical Information Service, Springfield, Virginia 22151

A FLIGHT EVALUATION OF METHODS FOR PREDICTING VORTEX WAKE EFFECTS ON TRAILING AIRCRAFT

Glenn H. Robinson and Richard R. Larson
Flight Research Center

INTRODUCTION

The introduction of heavy jet transport aircraft into commercial service has renewed interest in vortex wake phenomena, particularly because the wakes from such aircraft are potentially hazardous to small aircraft that may encounter them. In the interest of promoting greater safety in areas of mixed air traffic, the National Aeronautics and Space Administration was requested by the Federal Aviation Administration to evaluate in flight the vortex wake effects generated by large jet aircraft and to assess the adequacy of current methods for predicting such effects. The results of the flight evaluation, which encompassed a fairly broad range of aircraft sizes and combinations, were summarized in reference 1.

This study compares the results from reference 1 with the wake effects predicted by several analytic methods in an effort to develop a reliable technique for estimating minimum separation distances between aircraft of various sizes. Four analytic expressions currently used to define the strength and persistence of vortex flow are considered. The maximum rolling moment predicted by each method for trailing aircraft at various separation distances from the generating aircraft is compared with corresponding flight data from reference 1 for various combinations of leading and trailing aircraft. A modified analytic expression, which best represents the available flight data, is derived and used to estimate the hazards of vortex wake encounters.

SYMBOLS

Physical quantities in this report are given in the International System of Units (SI) and parenthetically in U.S. Customary Units. The measurements were taken in Customary Units. Factors relating the two systems are presented in reference 2.

b, $\bar{b}$	wingspan of the generating and probe aircraft, respectively, m (ft)
b_v	distance between wingtip vortices, $\frac{\pi b}{4}$, for elliptic span loading (ref. 3), m (ft)
b_{v_f}	distance between flap outer-edge vortices, m (ft)
C_L	airplane lift coefficient, $\frac{L}{qS}$

C_l	rolling-moment coefficient
C_{l_p}	roll-damping derivative, per rad
C_{l_β}	dihedral derivative, per rad
C_{l_δ}	lateral-control-effectiveness derivative, per rad
c, $\bar{c}$	wing chord of the generating and probe aircraft, respectively, m (ft)
c_{av}	mean wing chord, S/b, m (ft)
c_l	section lift coefficient, $\frac{L'}{qc}$
c_{l_α}	section lift-curve slope, per rad
I_X	moment of inertia of probe aircraft about longitudinal axis, kg-m^2 (slug-ft^2)
J	gross weight per wingspan squared proportionality constant, kg/m^2 (lb/ft^2)
k	generalized viscosity constant, m^2/sec (ft^2/sec)
L	lift generated by wing, N (lb)
L'	lift per unit span, N/m (lb/ft)
p	roll rate, rad/sec
$\dot{p}$	roll acceleration, rad/sec^2
q	dynamic pressure, N/m^2 (lb/ft^2)
S, $\bar{S}$	wing area of the generating and probe aircraft, respectively, m^2 (ft^2)
t	vortex age, sec
V	true airspeed, knots or m/sec (ft/sec)
W	gross weight of generating aircraft, kg (lb)
w	vortex vertical velocity, m/sec (ft/sec)
y	horizontal distance through vortex velocity field, m (ft)
β	angle of sideslip, rad

Γ	vortex circulation, m^2/sec (ft^2/sec)
Γ_f, Γ_t	circulation strength of the flap and wingtip vortices, respectively, m^2/sec (ft^2/sec)
Γ_o	initial midspan vortex circulation, $\frac{4W}{\pi\rho Vb}$ or $\frac{2C_L VS}{\pi b}$ (level flight), m^2/sec (ft^2/sec)
Δy	incremental wingspan length, m (ft)
$\Delta\alpha$	incremental angle of attack, rad
δ	lateral control deflection, rad
ϵ	eddy viscosity constant, m^2/sec (ft^2/sec)
η	fractional semispan length
ν	kinematic viscosity constant, m^2/sec (ft^2/sec)
ρ	air density, kg/m^3 ($slugs/ft^3$)
Subscript:	
max	maximum

ANALYTIC CONSIDERATIONS

Three of the four analytic expressions considered in this study originated with reference 4, in which the radial distribution of velocity through a potential vortex (zero core size) is derived as a function of time. These expressions relate vortex vertical velocity at any radial distance, y, to the vortex circulation with initial strength, Γ_o, and have the following basic form:

$$w = \frac{\Gamma_o}{2\pi y}\left(1 - e^{-\frac{y^2}{4\nu t}}\right) \tag{1}$$

where ν is a measure of viscosity within the flow. Variations of this basic equation are shown as equations (2) to (4).

$$w = \frac{\Gamma_o}{2\pi y}\left(1 - e^{-y^2/4\nu t}\right) \quad \text{(ref. 5)} \tag{2}$$

where a value of $\nu = 0.2$ was used in this paper.

$$w = \frac{\Gamma_o}{2\pi y}\left[1 - e^{-y^2/4(\nu+\epsilon)t}\right] \quad \text{(refs. 6, 7)} \tag{3}$$

where values of $\epsilon = 0.0002\Gamma_o$ and $\nu = 0$ were used in this paper.

$$w = \frac{\Gamma_o}{2\pi y}\left[1 - e^{-y^2/\left(0.0042b^2 + 0.00012\frac{S\Gamma_o t}{b}\right)}\right] \text{ (ref. 8)} \qquad (4)$$

Each expression is identically proportional to vortex circulation. The expressions differ in the approach used for describing vortex decay as a function of time.

In equation (2) the viscous force is expressed as an "effective kinematic viscosity," using a simple constant from references 9 and 10 which approximates highly stable atmospheric conditions.

In equation (3) the viscous force is considered to be proportional to the shearing forces produced by both kinematic and eddy viscosity. Eddy viscosity, caused by small-scale turbulence within the vortex flow, is assumed to be dominant. Further, the eddy viscosity is assumed to be proportional to vortex circulation. The proportionality constant was determined experimentally by flying a Venom aircraft across wakes of Comet 3B and Vulcan 1 aircraft.

Similar assumptions relating eddy viscosity to generating aircraft wake circulation were used in the derivation of equation (4). In this study, flight measurements reported in references 6 and 11, and obtained by probing the wake of a Lincoln bomber and, independently, the wake of a P-51 Mustang fighter aircraft were used to determine the proportionality constant between eddy viscosity and circulation. A term proportional to the wingspan of the generating aircraft was also included in the calculations to attempt to account for initial vortex core size.

From a more current study of aircraft trailing vortex systems (ref. 12), which involved flight and wind-tunnel tests as well as analytical considerations, the following expression was derived:

$$w = \frac{\Gamma_o}{2\pi y}\left[0.16 + 0.16\log_e\left(3.91\frac{\pi^2 b}{S}\frac{y}{\sqrt{1 + 0.0065\frac{Vbt}{S}}}\right)\right] \text{(ref. 12)} \qquad (5)$$

This equation and the analysis from which it was obtained depart basically from equation (1) by suggesting that at full-scale Reynolds numbers vortex decay is not dependent on viscosity. Rather, the study shows that the circulation through the core of a turbulent vortex is proportional to the logarithm of the core radius. Further, the decay in maximum tangential velocity is shown to be an explicit function of downstream distance, while circulation at the core expressed as the product of maximum tangential velocity and core radius remains constant with downstream distance.

To illustrate the range of variability between the four expressions, figure 1(a) shows computed vertical-velocity profiles across a vortex wake 7.41 kilometers (4.0 nautical miles) behind a C-5A airplane. The flight conditions used in the calculations were a nominal gross weight of 204,120 kilograms (450,000 pounds), an indicated airspeed of 140 knots, and an altitude of 3810 meters (12,500 feet). The radius of the vortex core can be approximated as the horizontal distance from the vortex origin to the peak vertical-velocity point. Obviously, a short-span airplane in the wake vortex of the C-5A

airplane would be subject to major differences in vertical velocity, depending on the expression used.

Figure 1(b) illustrates the second primary variable: the change in vertical velocity with time, or, as shown, separation distance between the C-5A airplane and a following airplane. The calculations were based on equation (3).

The vortex centers in figure 1 were referenced to a common origin in the same vertical plane relative to the C-5A semispan.

In general, the wide variation in computations of vertical velocity and core radius emphasizes the sensitivity of these calculations to estimates of viscous decay within the vortex structure. Further, the viscous effects themselves are difficult to estimate, because they are dependent on meteorological parameters such as local wind gradients and temperatures experienced during a specific flight-test period.

Vortex-Induced Rolling Moments

By using the four equations and a spatial definition between the generator and probe aircraft like that shown in figure 2, vertical-velocity profiles were calculated for a number of conditions investigated during the flight tests reported in reference 1. Table 1 lists the flight conditions and the characteristics of the aircraft used in the study.

Vertical-velocity profiles across the right wingtip vortex, and including the left vortex contribution, were computed by using the following general expression developed in reference 5:

$$w(y) = \frac{\Gamma_o}{2\pi}\left[\frac{1}{y}\left(1 - e^{-y^2/kt}\right) - \frac{1}{y + b_v}\left(1 - e^{-(y+b_v)^2/kt}\right)\right] \qquad (6)$$

(Right vortex; Left vortex)

The computed vertical velocities were converted to a rolling-moment coefficient by instantaneously centering the probe airplane in the right-wingtip vortex of the generating airplane, thereby creating a spanwise change in angle of attack in terms of the vortex vertical-velocity profile as follows:

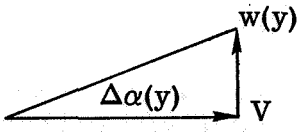

$$\Delta\alpha(y) \approx \frac{w(y)}{V}$$

This change in angle of attack produced, in turn, a rolling moment about the longitudinal axis. Thus

$$\text{Rolling moment} = \sum L(y)y$$

$$= \sum c_{l_\alpha} \Delta\alpha(y) q \bar{c}(y) y \Delta y$$

$$= c_{l_\alpha} \frac{q}{V} \sum_{-\bar{b}/2}^{\bar{b}/2} w(y) \bar{c}(y) y \Delta y \qquad (7)$$

and as a coefficient

$$C_l = \frac{\text{Rolling moment}}{q\bar{S}\bar{b}} = \frac{c_{l_\alpha}}{\bar{S}\bar{b}V}\sum_{-\bar{b}/2}^{\bar{b}/2} w(y)\bar{c}(y)y\Delta y \tag{8}$$

Vortex-Induced Rolling Moments Measured in Flight

The effect of the vortex wake on the trailing aircraft was usually determined by positioning the probe airplane slightly below the wake of the generating airplane's right wingtip and then climbing through the wake. Maximum angular roll acceleration, the corresponding roll rate, and the opposing lateral control input were measured each time it was determined that the probe aircraft had intersected the wake of the generating aircraft. (Reference 1 includes details of the flight-test procedure and examples of the data analyzed.)

The following single-degree-of-freedom expressions were used to extract rolling-moment coefficients from the roll excursions experienced by the probe airplane:

$$\underset{\text{Measured}}{I_X\dot{p}} = \underset{\text{Vortex induced}}{\text{Rolling moment}} + \underset{\text{Aircraft aerodynamics}}{q\bar{S}\bar{b}\left(C_{l_\delta}\delta + C_{l_\beta}\beta + \frac{\bar{b}}{2V}C_{l_p}p\right)} \tag{9}$$

Vortex-induced rolling-moment coefficient

$$C_l = \frac{I_X\dot{p}}{q\bar{S}\bar{b}} - \left(C_{l_\delta}\delta + \frac{\bar{b}}{2V}C_{l_p}p\right) \tag{10}$$

Equation (10) does not account for rolling moments introduced by yawing excursions of the probe aircraft. This contribution, although sometimes significant, was not included because it was not possible to differentiate between true airplane yaw and the transient sideslip vane response produced by the vortex flow angularity.

Span Load Distribution

Basically, the behavior of a trailing vortex system depends on the circulation pattern across the wingspan. The lift produced per unit of span is in turn related to the circulation at any point along the span, as stated by the Kutta-Joukowski theorem (ref. 13), that is,

$$L' = \rho V\Gamma \tag{11}$$

The relationships that link local circulation with the local lift at any spanwise station become (ref. 14):

$$L' = c_l cq \tag{12}$$

$$\Gamma = \frac{c_{\ell} cV}{2} \tag{13}$$

The total circulation in the trailing vortex system is then obtained from a spanwise summation of the circulation distribution across each half of the wing. Usually an elliptic spanwise lift distribution is assumed and the total circulation is given by the well-known relation

$$\Gamma_o = \frac{4L}{\pi \rho V b} \tag{14a}$$

$$\Gamma_o = \frac{2C_L VS}{\pi b} \tag{14b}$$

Although an elliptic loading assumption is generally satisfactory for a clean wing, the loadings for takeoff or landing configurations are far from elliptic, because of deflection of flaps, slats, spoilers, and other control devices which produce local changes in the spanwise loading.

RESULTS AND DISCUSSION

In the following sections the structure of the vortex wake and the rolling moment induced on several probe aircraft are considered for generating aircraft in both a clean-wing configuration and flaps-down configuration. Rolling moments calculated by using equations (2) to (5) are compared with available flight data for several combinations of generating and probe aircraft. A prediction method is developed that best describes the trend of the data, and is used to establish a criterion for estimating minimum separation distance.

Vortex Wake for a Clean-Wing Configuration

Span load distribution. – Calculated and wind-tunnel values of the spanwise distribution of loading and vorticity for the C-5A airplane in a clean-wing configuration are compared in figure 3. The load distribution (fig. 3(a)) was obtained from wind-tunnel pressure-distribution data and is compared with an elliptic span loading at the same angle of attack. The flight conditions for this example are $C_L = 0.81$ and $V = 229$ knots. The difference in overall circulation strength between the integrated wind-tunnel and elliptic span loadings is less than 3 percent.

The changes in trailing vortex strength due to differences in load distribution are illustrated further in figure 3(b) in terms of the distribution of vorticity within the wake streaming behind the wing. The vorticity, as discussed in detail in reference 15, is proportional to the slope of the span loading curve at each span station. Discrete vortices form along the span at the centroid of those areas which are bounded by zero, or low vorticity values. In this example, vorticity is concentrated near the wingtip and, to a small extent, at each engine pod location. Total vorticity, which is proportional to total area under either span loading curve, remains nearly the same. Specifically, vorticity contained within the tip vortex, $\eta \approx 0.8$ to 1.0, differs less than 1 percent

between the two load distribution curves.

Comparison of flight data with theory. – The example in the preceding section supports the assumption that spanwise loading on clean wings is elliptic, and that equation (14) is a valid representation of the circulation in the tip vortices of clean-wing configurations. On the basis of this assumption, rolling-moment coefficients were calculated as a function of separation distance, or vortex age, using equation (8) in conjunction with equations (2) to (5). Results for the various combinations of probe and generating airplanes investigated are shown in figures 4(a) to 4(f). For comparison with these results, the vortex-induced rolling-moment coefficients based on measured roll responses of the probe aircraft were calculated using equation (10). The comparison is made in terms of the ratio of the vortex-induced rolling moment to the maximum lateral control power available to the probe airplanes at each flight condition. Flight conditions and pertinent aerodynamic data are given in table 1.

The flight data show large variations in the rolling-moment ratios at similar separation distances. This variation reflects the difficulty of maneuvering the probe airplane so that it consistently intersected the trailing vortex core. Hence, for the purpose of comparing calculated and flight-measured rolling-moment ratios, each of the expressions was related conservatively to the uppermost boundary formed by the flight data. No single expression consistently provided an upper boundary compatible with the flight data. Rolling-moment ratios computed with equation (2) were usually about double the flight values. (See figure 4(a) for a representative comparison.) Consequently, this expression was eliminated. The best approximations of the upper limit were provided by equations (3) and (5); the rolling-moment ratios given by equation (4) were low. The vortex decay rate (decrease in rolling-moment ratio with increasing separation) of equation (5) is lower than for either equation (3) or equation (4).

To summarize, the maximum vortex-induced roll response obtained in flight from a fairly representative sample of probe and generating airplane combinations was approximately comparable to the roll response given by two of the four analytic expressions under consideration. Also, within a separation distance between the probe and generating airplanes of 14.8 to 18.5 kilometers (8.0 to 10.0 nautical miles), both the measured and computed maximum rolling moments generally exceeded the maximum lateral control power of the probe airplane.

Vortex Wake for Flaps-Down Configurations

Span load distribution. – Results of a parallel assessment of the analytical methods in relation to the flight data of reference 1 are given in figures 5 to 10 for various landing-flap configurations of the generating aircraft. Figure 5 illustrates the deviation from elliptic loading when wing flaps are deployed. Data were obtained from C-5A wind-tunnel pressure-distribution measurements, and the wing spanwise load distribution was determined for the power-approach configuration (25° flaps). Calculated values were computed for a flight condition corresponding to $C_L = 1.11$ at $V = 169$ knots. As shown in figure 5(a), the wind-tunnel and calculated values of total circulation strength in the trailing vortex differ less than 1.5 percent, based on the area beneath the span loading curves. However, the distribution of vorticity across the wingspan, shown in figure 5(b), differs markedly between the two span loading curves. The vorticity is concentrated near the inner and outer edges of the flap and near the wingtip. Separate vortices form

at these locations, with the vortex at the flap inboard edge rotating counter to the two outboard vortices. Approximately 14 percent of the total vorticity is distributed from the centerline to $\eta \approx 0.675$, an additional 46 percent is produced at the flap outer edge ($\eta \approx 0.675$ to 0.840), and the remaining 40 percent is produced at the wingtip. The hazard to small following aircraft is reduced at the flap inner edge vortex ($\eta \approx 0.17$) by the adjoining counterrotating vortex on the opposite wing panel, but the two corotating vortices near the wingtip ($\eta \approx 0.77$, 0.98) remain a hazard.

The individual vertical-velocity profiles of the two corotating vortices near the wingtip are shown in figure 6. The profiles were calculated for a separation distance of 1.85 kilometers (1.0 nautical mile) using equation (6) modified as follows to account for the vortex at the flap outboard edge:

$$w(y) = \frac{\Gamma_t}{2\pi}\left[\underbrace{\frac{1}{y}\left(1 - e^{-y^2/kt}\right)}_{\text{Right-tip vortex}} - \underbrace{\frac{1}{y + b_v}\left(1 - e^{-(y+b_v)^2/kt}\right)}_{\text{Left-tip vortex}}\right]$$

$$+ \frac{\Gamma_f}{2\pi}\left\{\underbrace{\frac{1}{y + \left(\frac{b_v}{2} - \frac{b_{v_f}}{2}\right)}\left[1 - e^{-\left(y+\frac{b_v}{2}-\frac{b_{v_f}}{2}\right)^2/kt}\right]}_{\text{Right-flap vortex}} - \underbrace{\frac{1}{y + \left(\frac{b_v}{2} + \frac{b_{v_f}}{2}\right)}\left[1 - e^{-\left(y+\frac{b_v}{2}+\frac{b_{v_f}}{2}\right)^2/kt}\right]}_{\text{Left-flap vortex}}\right\} \tag{15}$$

where Γ_f and Γ_t are the circulation strengths of the flap and wingtip vortices determined from the corresponding areas under the vorticity distribution curve and b_{vf} is the flap vortex span. Although this simple linear model fails to account for coupling between the velocity components, it does give some insight into the vortex structure. In particular, a canceling effect is shown in the vertical velocity between the vortex cores. The magnitude of this canceling effect is a simple function of the vertical-velocity gradient across each vortex core and the distance between cores. The effect, reported in reference 6, is further illustrated in figures 7(a) to 7(c), in which vertical-velocity profiles are presented for separation distances of 1.85, 5.56, and 9.26 kilometers (1.0, 3.0, and 5.0 nautical miles). As shown, the attenuating effect diminishes with time and eventually approaches the single vortex representation.

Comparison of flight data with theory. – The flight condition used in the calculations for figures 5 to 7 was taken from one of the flight-test series reported in reference 1. In figure 8 the flight-test data obtained during this series are presented with corresponding analytic curves for the single and the double vortex wake system. For the double

vortex system, each corotating vortex was assumed to precess about the other so that the two vortices followed a path around a rotation point midway between them. The probe airplane, a Learjet 23, was positioned at this midpoint location. (See references 6, 15, 16, and 17 for detailed analyses of multiple vortex systems.) The data are presented as the ratio of the coefficient of the rolling moment induced by the vortex wake to the maximum lateral control power of the probe airplane at the flight condition investigated. This ratio is plotted as a function of the separation distance between the aircraft.

Figure 8 shows that the magnitude of the roll excursions experienced by the Learjet 23 varied widely and in one instance exceeded three times the available roll control power. On the basis of figure 7(a), the Learjet 23 airplane, with a wingspan of 10.4 meters (34.1 feet), could be totally immersed in the C-5A wake, making the roll response of this short-span airplane particularly sensitive to the vortex circulation.

Recent studies indicate the vortex structure to be comprised of strongly coupled circumferential and axial flows which greatly affect the distribution of lift on an aircraft penetrating the wake (refs. 18 to 20). The large variation in the magnitude of the calculated rolling moments shown in figure 8 further illustrates the sensitivity of the short-span aircraft to even the simple changes in velocity gradient considered herein.

The Cessna 210 and the F-104 aircraft are also sensitive to large aircraft wakes. Both of these short-span aircraft were used in reference 1 to probe the C-5A wake, although only limited quantitative data were obtained with the Cessna 210 airplane. The F-104 airplane, which has a wingspan of 6.7 meters (22.0 feet), experienced the most violent roll upsets in the program. (See reference 1, figures 3(a), 3(d), 3(e).)

In figure 8 for a separation distance of approximately 13.0 kilometers (7.0 nautical miles), the single vortex model represented by equation (5) is in best agreement with the flight measurements, which conflicts with the preceding span load analysis. However, for the double vortex solution, the probe airplane was positioned midway between the two vortices. As shown in figure 9, if the probe airplane had been displaced laterally toward either the flap or wingtip vortex, the rolling-moment ratios would have been somewhat closer to the flight measurements. Even then, however, the peak flight values of rolling-moment ratio shown in figure 8 are twice the maximum calculated value.

Figures 10(a) and 10(b), together with figure 8, illustrate the effect of the C-5A wake on progressively larger aircraft. In general, the maximum rolling excursions experienced by the McDonnell-Douglas DC-9 and Convair 990 airplanes, although of less magnitude than that experienced by the Learjet 23 airplane, still exceeded the available roll control power at separation distances less than approximately 9 and 5 kilometers (5 and 3 nautical miles), respectively. The influence of the double vortex wake on the rolling moments of the larger probe aircraft is proportionally less, which suggests that the vortex structure created by the flap and tip vortices has less influence on the overall lift distribution of the larger probe aircraft.

Although these limited flight measurements do not establish the validity of the double vortex model, pilots consistently described the wake produced during flaps-down tests as less coherent, less well defined, and of larger diameter than the wake from the clean-wing tests.

Figures 10(c) and 10(d) complete the comparison of flight measurements with

theoretical estimates. For these comparisons, the calculated curves are based on elliptic loading and equation (14), because of the lack of span load distribution data for the generating airplane. The figures again illustrate the relative effect produced on a small and a large probe airplane when subjected to a vortex of common size and strength.

From the data presented, it appears that for both clean and flaps-down wing configurations, equation (3) and equation (5) provide conservative estimates of vortex strength and decay with time as compared with the flight-test results, and equation (4) gives low estimates of vortex strength. In the critical separation range for terminal operations (approximately 4 to 9 kilometers (2 to 5 nautical miles)), vortex strength may be overestimated for landing-flap configurations if the computations are based exclusively on elliptic span loading. More realistic estimates of vortex strength will result from detailed analytic and experimental studies of multivortex systems. The simple analytic models of vortex structure considered herein, when applied to small airplanes with wingspans near the vortex core diameter, were particularly deficient in representing the induced airloads and moments on the probe aircraft.

Estimation of Minimum Separation Distance

An assessment of vortex strength independent of the measured probe airplane response was obtained from the program pilots who were asked to establish a minimum safe separation distance for each test series. The assessment was made considering the structural integrity of the probe airplane, passenger comfort, possible loss of control during IFR flight conditions, and the hazards of maneuvering close to the ground. This information was particularly useful because the pilots were best able to evaluate each roll upset relative to the degree with which the airplane was centered in the wake. The pilot assessment of minimum separation distance is compared in figures 11(a) and 11(b) with distances calculated with equations (3) and (4) for all the combinations of probe and generating airplanes considered in figures 4 and 8. The minimum separation distance was arbitrarily defined as that distance where the rolling moment computed by each analytic expression was equal to the maximum available lateral control power ($\frac{C_l}{C_{l_\delta}\delta_{max}} = 1$). The two flagged points shown in the figures were not included in the flight tests, thus 18.5 kilometers (10.0 nautical miles) is an estimated minimum separation distance based on excursions experienced when the airplanes were tested in the landing configuration.

Figure 11(a) compares the pilot assessment with vortex decay rates calculated with equation (4). The figure shows, again, that equation (4) underpredicts vortex activity. An opposite trend is shown in figure 11(b), in which the pilot assessment is compared with calculated vortex decay rates from equation (3). In this instance, the calculated minimum separation distance is conservative.

On the basis of the maximum lateral control power criteria, decay rates computed with equation (5) produced excessively large separation distances; thus this equation was eliminated from the remaining analysis.

Relationship to wingspan ratio. – The ratio of probe airplane to generating airplane wingspan has been used as a correlating parameter of vortex interference for various airplane combinations (ref. 6, for example). References 21 to 23 also suggest wingspan

ratio as the pertinent parameter for defining vortex hazard. In essence, these studies assumed that a vortex encounter would not be dangerous when the maximum steady roll capability of the probe aircraft exceeded the circulation around the vortex. Expressed algebraically,

$$(\Gamma_o)_{\text{generating airplane}} < \frac{\pi}{2}\left(p_{max}\bar{b}^2\right)_{\text{probe airplane}} \tag{16}$$

A relationship between the gross weight and wingspan of the generating aircraft may be generalized as

$$W = Jb^2 \tag{17}$$

where $J \approx 24$ to 98 kg/m^2 (5 to 20 lb/ft^2) for a fairly large sample of conventional aircraft configurations. Also, as a single-degree-of-freedom approximation, maximum roll rate may be expressed as

$$p_{max} \approx -\frac{C_{l_\delta}\delta_{max}}{C_{l_p}}\frac{2V}{\bar{b}} \tag{18}$$

By using these equations, an expression can be derived which defines aircraft combinations capable of producing a vortex hazard to the trailing aircraft. This expression, formed by simple substitution of equations (14a), (17), and (18) into the inequality (eq. (16)), simplifies to

$$\frac{2J}{\pi^2} < \frac{q}{b}\left(-\frac{C_{l_\delta}\delta_{max}}{C_{l_p}}\bar{b}\right)_{\text{probe airplane}} \tag{19}$$

The expression is plotted in figure 12 versus wingspan ratios for all the aircraft combinations considered. As shown, wingspan ratio is the predominant variable, with the aerodynamic terms of the expression providing essentially linear scaling. The figure shows the change in the threshold between safe and hazardous separation as the size and wing loading of the generating airplane progresses from a light airplane ($J \approx 24$ kg/m^2 (5 lb/ft^2)) to a jumbo jet ($J \approx 98$ kg/m^2 (20 lb/ft^2)).

In figure 13 minimum separation distances calculated with equations (3) and (4) (as presented, and as expanded for flaps-down configurations as in equation (15)) are plotted against the wingspan-ratio parameter. The trend produced by equation (4) generally underestimates the current minimum separation distance required by the Federal Aviation Administration for terminal operations (ref. 24), whereas equation (3) generally overestimates it. More important, both equations show that separation distances should be increased as the wingspan ratio increases, when most evidence indicates the opposite.

Modified vortex velocity equation. – A detailed comparison of the vortex-induced rolling-moment trends predicted by equations (3) and (4) with the maximum flight-measured rolling moments reveals that a simple interpolation between the two equations as functions of wingspan ratio provides a reasonable fit with most of the flight data. Both equations were originally derived by semiempirical methods from common flight-test results, so a linear interpolation does not violate the assumptions or basic relations

used in the derivations. On the basis of these considerations, the following relationship was derived for wingspan ratios from approximately 0.1 to 0.8:

$$w_{(\text{interpolated})} = \frac{\Gamma_o}{2\pi y}\left\{1 - \left[A_1 e^{-y^2/0.0008\,\Gamma_o t} + A_2 e^{-y^2/(0.0042b^2+0.00012\,c_{av}\Gamma_o t)}\right]\right\} \tag{20}$$

where

$$A_1 = 1 - A_2$$

$$A_2 = 1.66\bar{b}/b - 0.259$$

Figures 14(a) to 14(k) combine the flight data from figures 4 and 8, the pilot assessment of the minimum separation distance, and the rolling-moment-ratio curves calculated by using equation (20). The interpolated curves form a fairly representative upper boundary, except for the combinations of probe and generating aircraft with the lowest wingspan ratios. For these combinations, as shown in figure 14(g), much larger roll upsets could be experienced.

To assess the validity of equation (20) and maximum lateral control power as criteria for establishing minimum separation distance, the calculated minimum separation is correlated with the pilot assessments and wingspan ratio in figure 15. Although the data are scattered, figure 15(a) shows the proposed criterion to be fairly representative of the pilot assessment. Figure 15(b) shows the proposed criterion to be somewhat conservative relative to the current criterion of reference 24, for separation distances greater than approximately 9 kilometers (5.0 nautical miles), that is, wingspan ratios less than 0.5. The proper trend of increasing separation distance with decreasing wingspan ratio is established, however. For airplane combinations with wingspan ratios less than about 0.2, separation distances should be greater than that given by equation (20).

Figure 16 compares the minimum separation distance calculated with equation (20) with the vortex hazard expression derived in equation (19). Although there is scatter in the data, this summary indicates that about half the combinations tested would experience vortex-induced rolling moments in excess of available roll control power. This number is somewhat less conservative than the number of combinations requiring increased separation based on the wingspan ratio relationship (fig. 15(b)). Both methods, however, indicate that the greatest hazard exists for aircraft combinations with wingspan ratios less than about 0.4 to 0.5.

CONCLUDING REMARKS

Rolling moments induced on several probe aircraft by the vortex wake from large transport aircraft were calculated with four analytic expressions and the results compared with flight data for corresponding combinations of generating and probe aircraft. No single expression consistently predicted the magnitude of the induced rolling moments experienced in flight. A simple interpolation between two of the expressions, however, provided an empirical expression which could be used to estimate minimum safe

separation distances. This expression was applied successfully to probe and generating airplane combinations with wingspan ratios in the range from 0.3 to 0.8, but tended to underestimate the induced effects on small aircraft that would be completely immersed in one of the rolled-up vortices.

In general, the maximum induced rolling moments exceeded the lateral control power of most of the probe aircraft considered within minimum separation distances normally maintained during landing and takeoff operations.

Flight Research Center,
National Aeronautics and Space Administration,
Edwards, Calif., June 20, 1972.

REFERENCES

1. Andrews, William H.; Robinson, Glenn H.; and Larson, Richard R.: Exploratory Flight Investigation of Aircraft Response to the Wing Vortex Wake Generated by Jet Transport Aircraft. NASA TN D-6655, 1972.

2. Mechtly, E. A.: The International System of Units – Physical Constants and Conversion Factors. NASA SP-7012, 1969.

3. Spreiter, John R.; and Sacks, Alvin H.: The Rolling Up of the Trailing Vortex Sheet and Its Effect on the Downwash Behind Wings. J. Aeron. Sci., vol. 18, no. 1, Jan. 1951, pp. 21-72.

4. Lamb, Horace: Hydrodynamics. Sixth ed., Dover Publications, Inc., 1932, p. 592.

5. Thelander, J. A.: Separation Minimums for Aircraft Considering Disturbances Caused by Wake Turbulence. Jan. 15, 1969. (Available from FAA Public Documents Inspection Facility, Wash., D. C.)

6. Kerr, T. H.; and Dee, F. W.: A Flight Investigation Into the Persistence of Trailing Vortices Behind Large Aircraft. Tech. Note Aero. 2649, Roy. Aircraft Establishment, Sept. 1959.

7. Rose, R.; and Dee, F. W.: Aircraft Vortex Wakes and Their Effects on Aircraft. Tech. Note Aero. 2934, Roy. Aircraft Establishment, Dec. 1963.

8. Wetmore, Joseph W.; and Reeder, John P.: Aircraft Vortex Wakes in Relation to Terminal Operations. NASA TN D-1777, 1963.

9. Bennett, W. J.: Analytical Determination of the Velocity Fields in the Wakes of Specified Aircraft. Rep. No. RD-64-55, FAA, May 1964.

10. Bennett, W. J.: State-of-the-Art Survey for Minimum Approach, Landing, and Takeoff Intervals as Dictated by Wakes, Vortices, and Weather Phenomena. Rep. No. RD-64-4, FAA, Jan. 1964.

11. Kraft, Christopher C., Jr.: Flight Measurements of the Velocity Distribution and Persistence of the Trailing Vortices of an Airplane. NACA TN 3377, 1955.

12. McCormick, B. W.; Tangler, J. L.; and Sherrieb, H. E.: Structure of Trailing Vortices. J. Aircraft, vol. 5, no. 3, May-June 1968, pp. 260-267.

13. Kuethe, A. M.; and Schetzer, J. D.: Foundations of Aerodynamics. Second ed., John Wiley & Sons, Inc., 1964.

14. Silverstein, Abe; Katzoff, S.; and Bullivant, W. K.: Downwash and Wake Behind Plain and Flapped Airfoils. NACA Rep. 651, 1938.

15. Bleviss, Z. O.: Theoretical Analysis of Light Plane Landing and Take-Off Accidents Due to Encountering the Wakes of Large Airplanes. Rept. No. SM-18647, Douglas Aircraft Co., Inc., 1954.

16. Hackett, J. E.; and Evans, M. R.: Vortex Wakes Behind High-Lift Wings. J. Aircraft, vol. 8, no. 5, May 1971, pp. 334-340.

17. Caiger, B.; and Gould, D. G.: An Analysis of Flight Measurements in the Wake of a Jet Transport Aircraft. J. H. Olsen, A. Goldburg, and M. Rogers, eds., Aircraft Wake Turbulence and Its Detection. Plenum Press, 1971, pp. 125-136.

18. Jones, W. P.; and Rao, B. M.: Airloads and Moments on an Aircraft Flying Over a Pair of Inclined Trailing Vortices. J. H. Olsen, A. Goldburg, and M. Rogers, eds., Aircraft Wake Turbulence and Its Detection. Plenum Press, 1971, pp. 523-545.

19. Batchelor, G. K.: Axial flow in trailing line vortices. J. Fluid Mech., vol. 20, part 4, 1964, pp. 645-658.

20. Chigier, N. A.; and Corsiglia, V. R.: Wind-Tunnel Studies of Wing Wake Turbulence. AIAA Paper No. 72-41, Jan. 1972.

21. Condit, P. M.; and Tracy P. W.: Results of the Boeing Company Wake Turbulence Test Program. J. H. Olsen, A. Goldburg, and M. Rogers, eds., Aircraft Wake Turbulence and Its Detection. Plenum Press, 1971, p. 494.

22. Goldburg, Arnold; Crow, Steven C.; Owen, Paul R.; Luffsey, Walter S.; Donaldson, Coleman duP.; and Chigier, Norman N.: Panel Discussion. J. H. Olsen, A. Goldburg, and M. Rogers, eds., Aircraft Wake Turbulence and Its Detection. Plenum Press, 1971, p. 579.

23. Anon.: FAA Symposium on Turbulence. FAA, March 24, 1971. (Available from NTIS as AD 732117.) .

24. Anon.: Procedures For Control of Aircraft Following Heavy Jet Aircraft. FAA Order 7110.29, Aug. 1971.

TABLE 1. SUMMARY OF AIRCRAFT CHARACTERISTICS AND FLIGHT CONDITIONS

(a) Wing area and wing span

Aircraft	S, m^2 (ft^2)	b, m (ft)
C-5A	576.0 (6200.0)	66.75 (219.0)
Convair 990	209.0 (2250.0)	35.97 (118.0)
DC-9	86.8 (934.0)	27.25 (89.4)
Learjet 23	21.6 (232.0)	10.39 (34.1)
Cessna 210	16.3 (175.5)	11.16 (36.6)

(b) Generating aircraft

Figure	Aircraft	Flap setting, deg	W, kg (lb)	Airspeed, KIAS
4(a), 14(a)	C-5A	0	274.8 to 279.0×10^3 (605.9 to 615.1×10^3)	190
10(b), 14(i)	C-5A	25	271.2 to 272.9 (598.0 to 601.7)	150
4(b), 14(b)	C-5A	0	273.7 to 278.5×10^3 (603.5 to 614.0×10^3)	190
10(a), 14(h)	C-5A	40	267.6 to 272.2 (590.0 to 600.0)	150
4(c), 14(c)	Convair 990	0	91.4 to 92.4×10^3 (201.4 to 203.6×10^3)	180
10(d), 14(k)	Convair 990	36	87.0 to 88.1 (191.7 to 194.3)	150
4(d), 14(d)	Convair 990	0	91.1 to 92.4×10^3 (200.8 to 203.7×10^3)	200
10(c), 14(j)	Convair 990	36	88.5 to 90.8 (195.1 to 200.2)	150
4(e), 14(e)	DC-9	0	32.1 to 33.1×10^3 (70.8 to 73.0×10^3)	200
8, 14(g)	C-5A	25	202.9 to 208.0 (447.3 to 458.6)	140
4(f), 14(f)	Convair 990	0	72.3 to 73.8×10^3 (159.3 to 162.8×10^3)	170

(c) Probe aircraft

Figure	Aircraft	Flap setting, deg	W, kg (lb)	Airspeed, KIAS	I_X, $kg\text{-}m^2$ ($slug\text{-}ft^2$)	C_{l_α}, 1/rad	$C_{l_\delta}{}_{max}$	C_{l_p}, 1/rad	Test altitude, m (ft)	q, N/m^2 (lb/ft^2)
4(a), 14(a)	Convair 990	0	75.7 to 77.1×10^3 (167.0 to 170.0×10^3)	190	2.64 to 2.67×10^6 (1.95 to 1.97×10^6)	5.67	0.0465	-0.406	3.81×10^3	5817.4 (121.5)
10(b), 14(i)	Convair 990	27	72.9 to 75.2 (160.7 to 165.7)	150	2.58 to 2.63 (1.90 to 1.94)		.0589	-.350	(12.5×10^3)	3610.2 (75.4)
4(b), 14(b)	DC-9	0	31.1 to 35.8×10^3 (68.5 to 78.9×10^3)	190	0.491 to 0.495×10^6 (0.362 to 0.365×10^6)	5.82	0.0442	-0.433		5817.4 (121.5)
10(a), 14(h)	DC-9	30 (gear down)	29.8 (65.7)	150	.407 (.300)		.0650	-.46		3610.2 (75.4)
4(c), 14(c)	DC-9	0	31.1 to 32.8×10^3 (68.5 to 72.4×10^3)	180	0.491 to 0.502×10^6 (0.362 to 0.370×10^6)	5.82	0.0461	-0.433		5171.1 (108.0)
10(d), 14(k)	DC-9	50 (gear down)	30.4 to 31.8 (67.0 to 70.0)	150	.447 to .495 (.330 to .365)		.085	-.460		3610.2 (75.4)
4(d), 14(d)	Learjet 23	0	5.2×10^3 (11.5×10^3)	200	0.0252×10^6 (0.0186×10^6)	5.21	0.0472	-0.410		6368.1 (133.0)
10(c), 14(j)	Learjet 23	38	5.2 (11.5)	150	.0252 (.0186)		.0455	-.410		3610.2 (75.4)
4(e), 14(e)	Learjet 23	0	5.2×10^3 (11.5×10^3)	200	0.0252×10^6 (0.0186×10^6)	5.21	0.0472	-0.410		6368.1 (133.0)
8, 14(g)	Learjet 23	20	5.2 (11.5)	140	.0252 (.0186)		.0463	-.410		3155.3 (65.9)
4(f), 14(f)	Cessna 210	0	1.4×10^3 (3.0×10^3)	130	0.00178×10^6 (0.00131×10^6)	5.11	0.0560	-0.480	2.9 (9.5)	2710.0 (56.6)

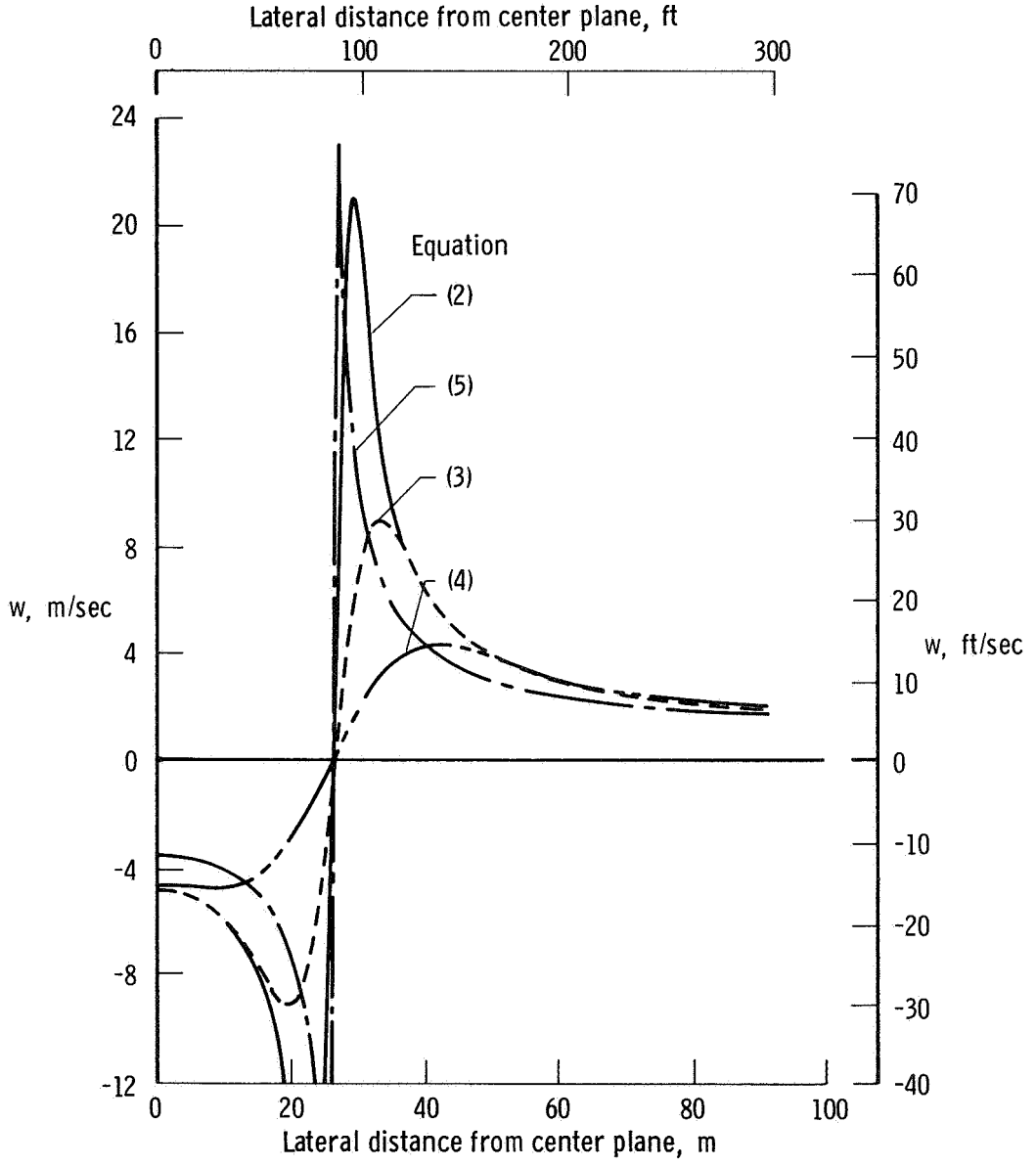

(a) Vertical-velocity profiles computed with four expressions for a separation distance of 7.41 kilometers (4.0 nautical miles).

Figure 1. Computed variation of C-5A vortex wake vertical velocity with lateral distance and time. Airspeed = 140 KIAS; W = 204,120 kilograms (450,000 pounds); altitude = 3810 meters (12,500 feet).

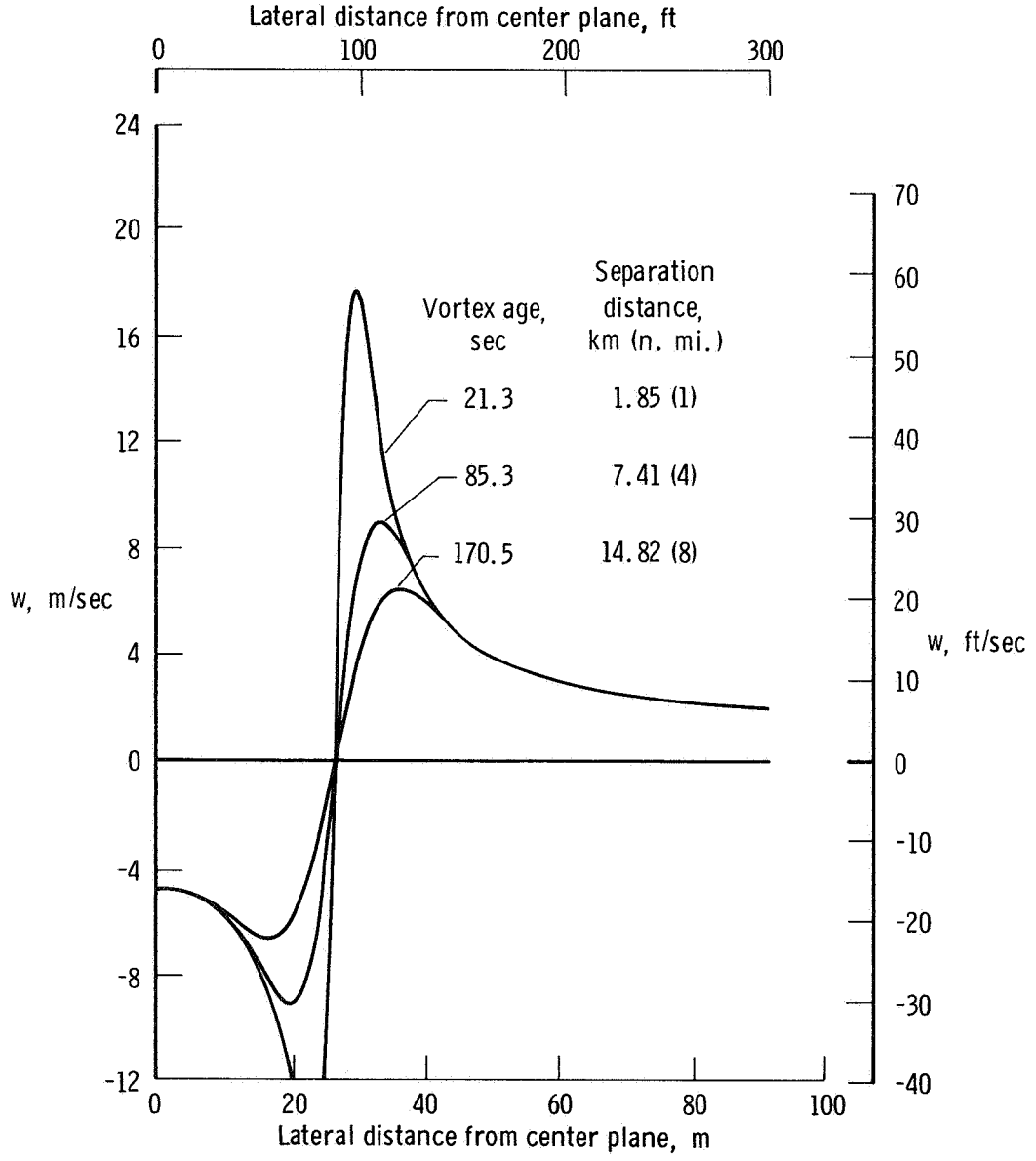

(b) Vertical-velocity profiles as computed with equation (3) for three separation distances.

Figure 1. Concluded.

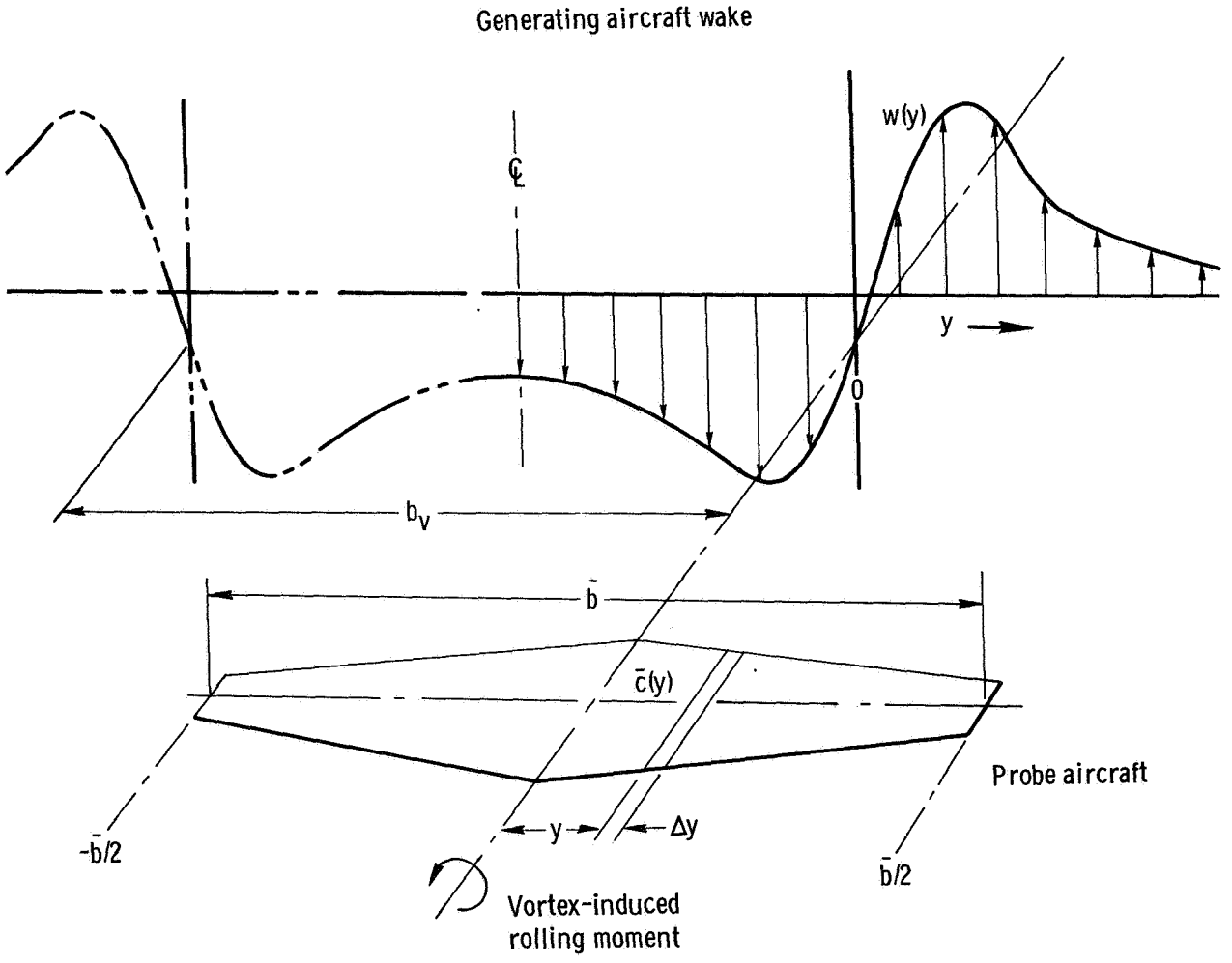

Figure 2. Spatial coordinates between probe and generating aircraft used in rolling-moment computation.

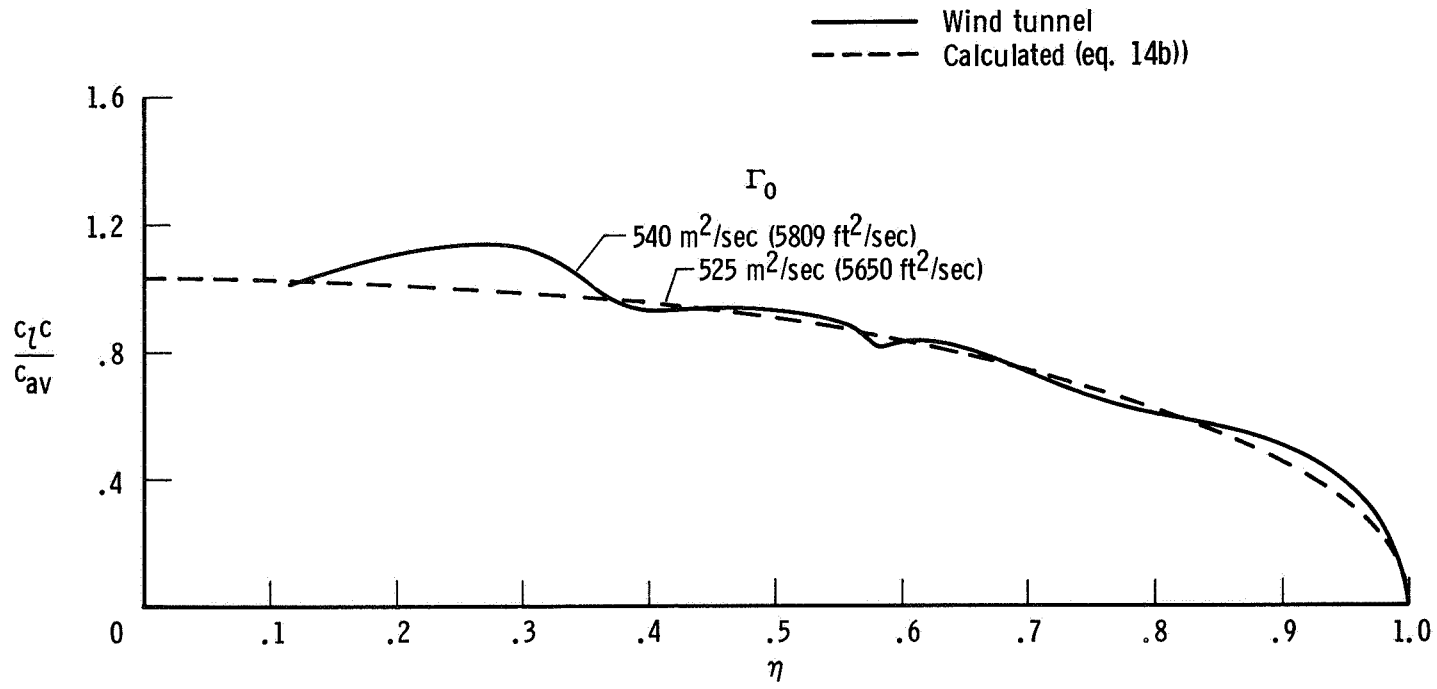

(a) Span load distribution.

Figure 3. Calculated and wind-tunnel values of span load and vorticity distribution for the C-5A airplane in the clean configuration. $C_L = 0.81$; V = 229 knots.

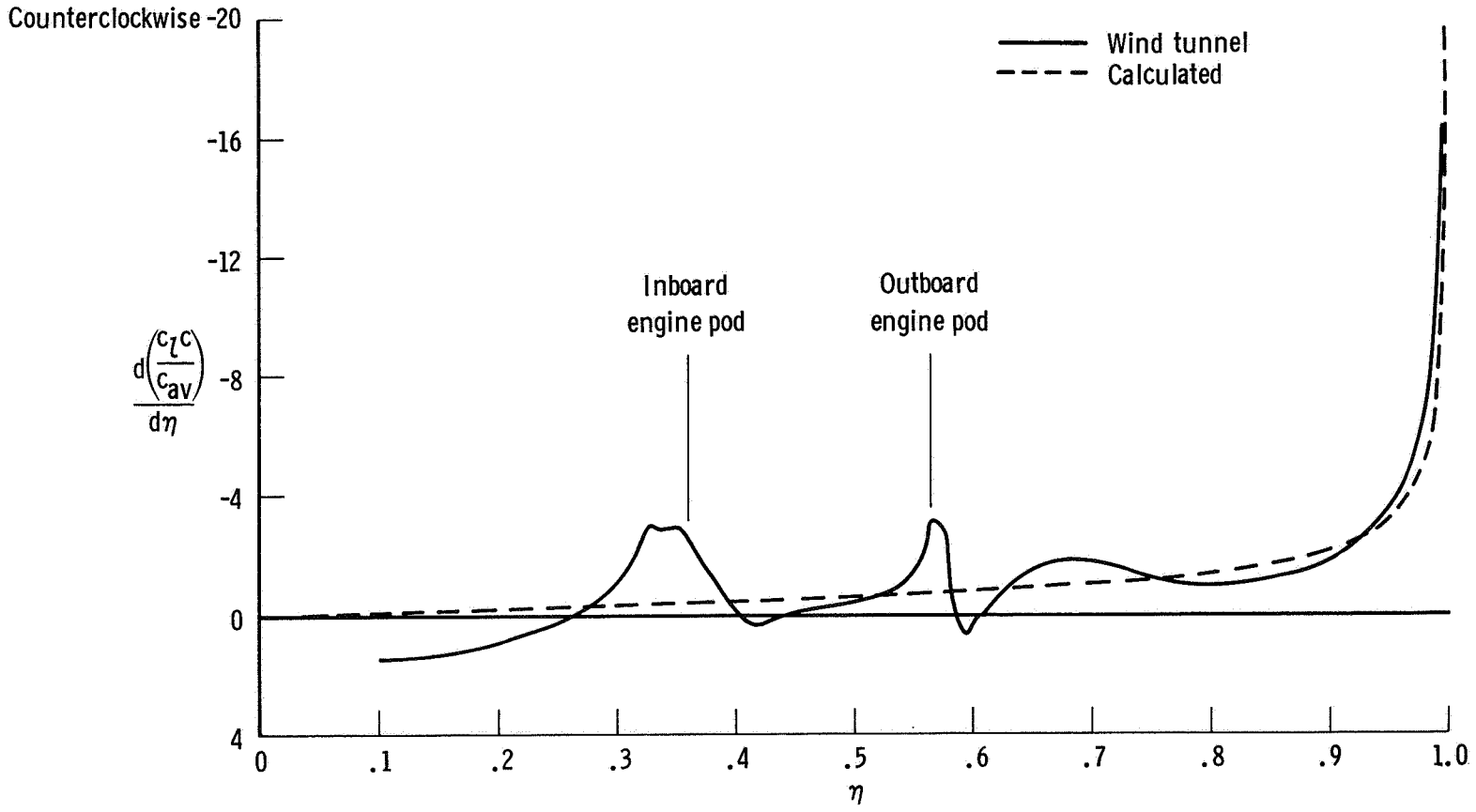

(b) Vorticity distribution.

Figure 3. Concluded.

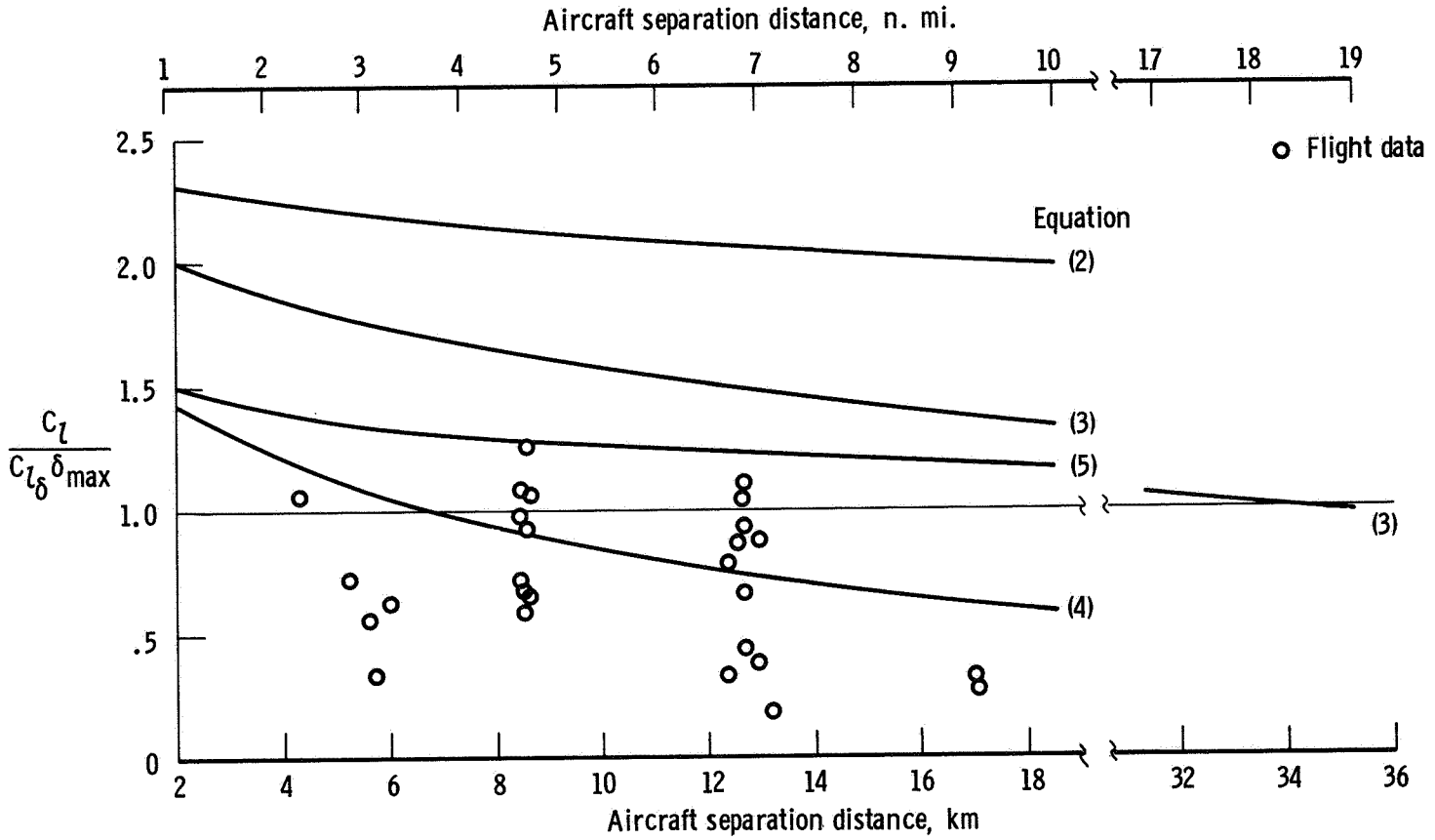

(a) Probe airplane: Convair 990, V = 229 knots, $C_{l_\delta \delta_{max}} = 0.0465$; generating airplane: C-5A.

Figure 4. Comparison of calculated and flight-test rolling-moment ratios for several probe and generating aircraft combinations. Clean-wing configuration.

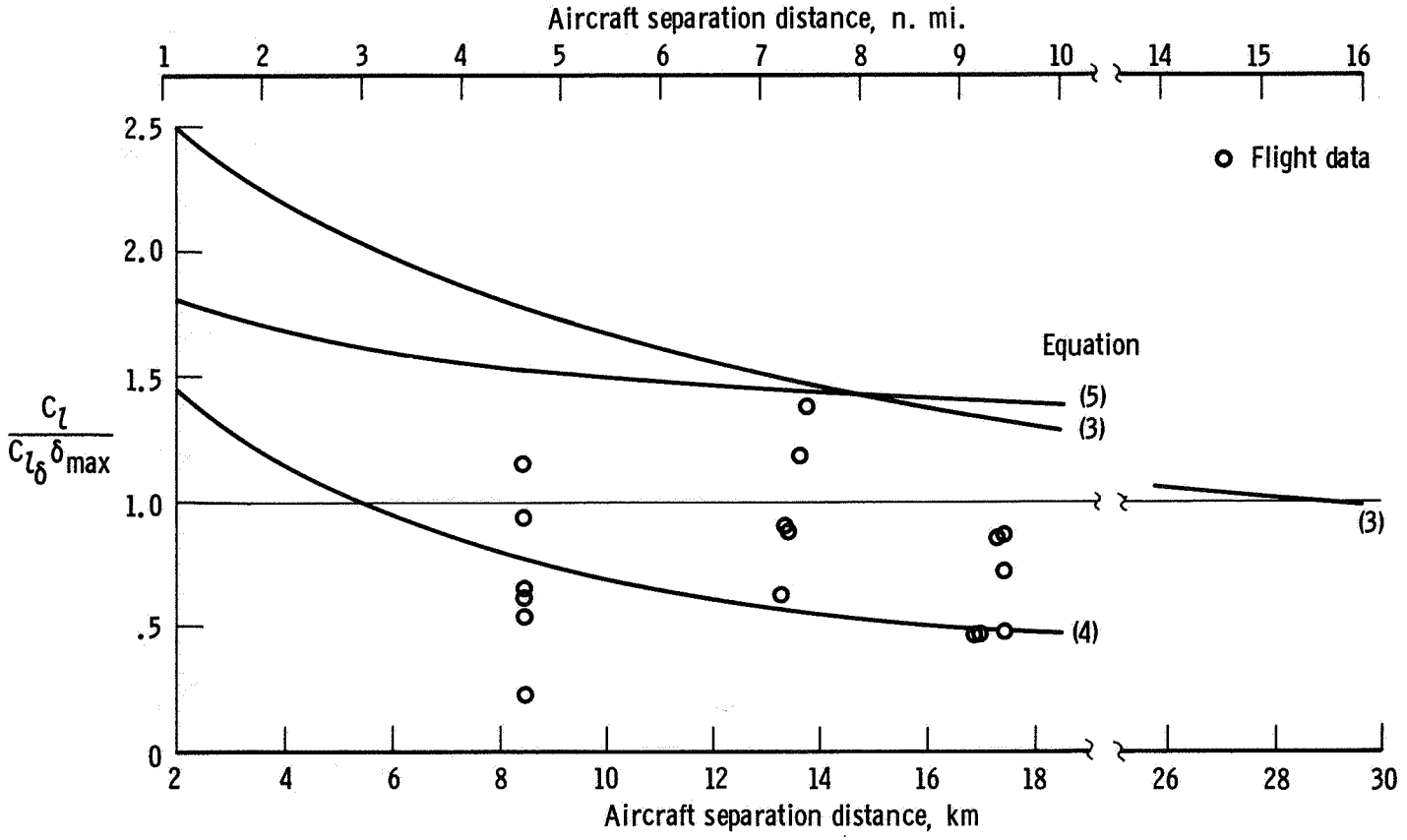

(b) Probe airplane: DC-9, V = 229 knots, $C_{l_\delta \delta_{max}} = 0.0442$; generating airplane: C-5A.

Figure 4. Continued.

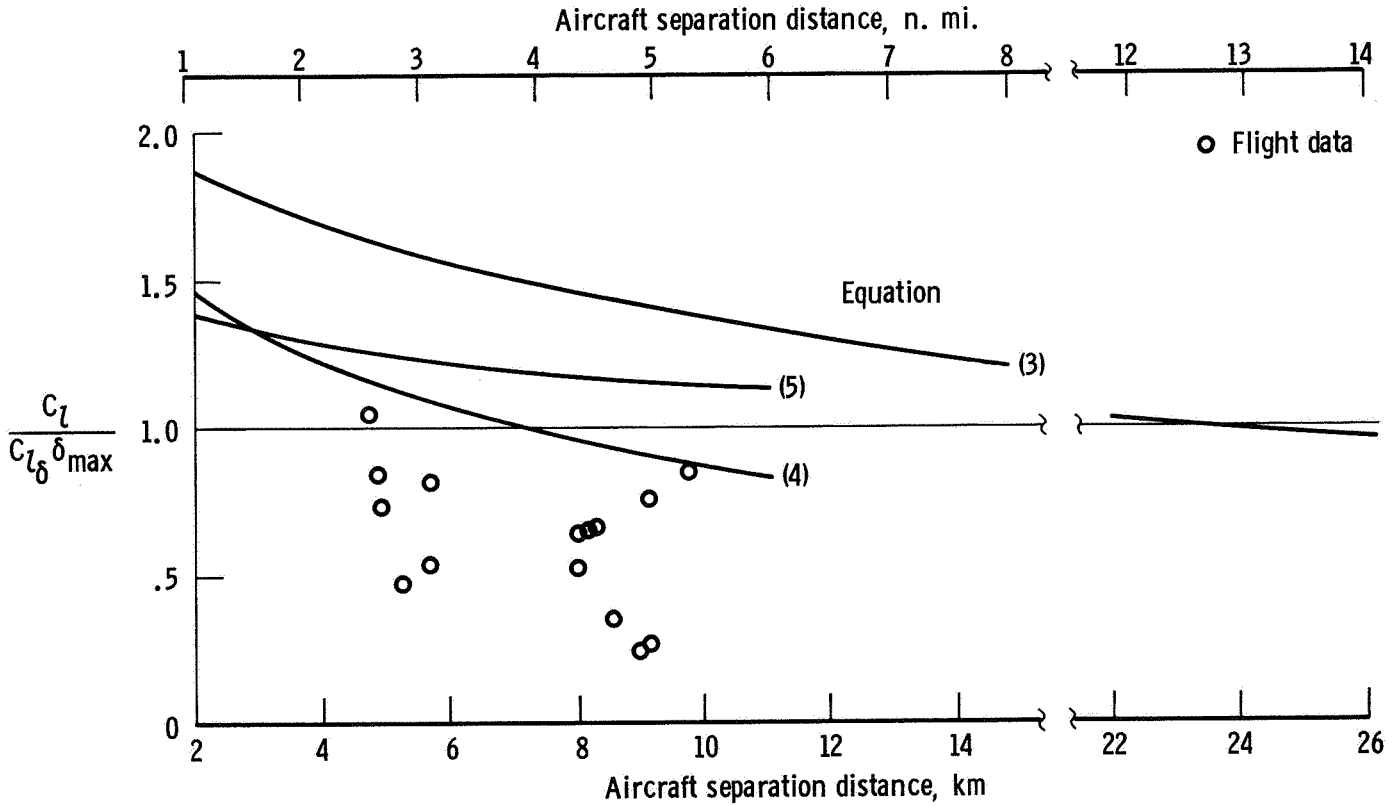

(c) Probe airplane: DC-9, V = 216 knots, $C_{l_\delta}{}_{\delta_{max}} = 0.0461$; generating airplane: Convair 990.

Figure 4. Continued.

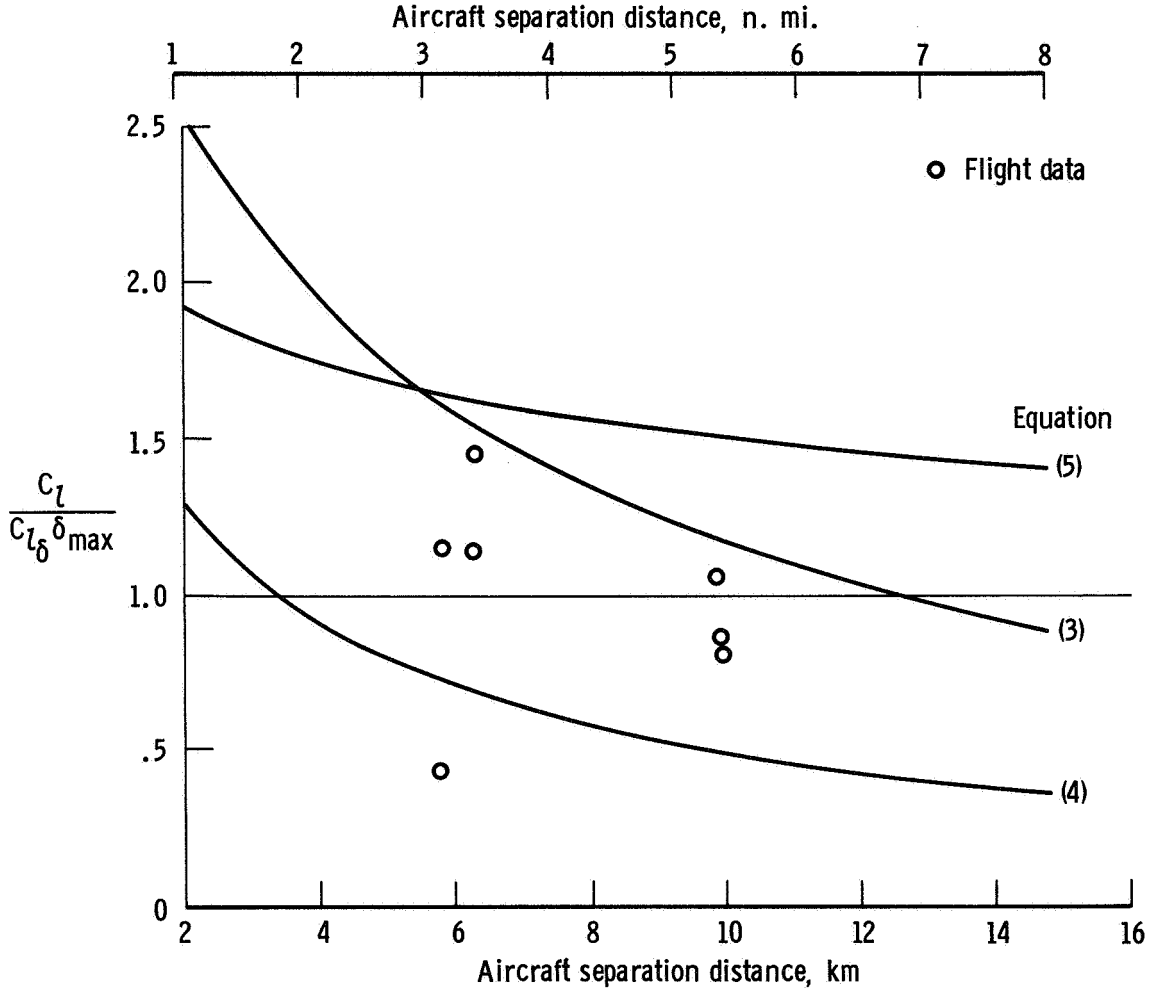

(d) Probe airplane: Learjet 23, V = 240 knots, $C_{l_\delta \delta_{max}} = 0.0472$; generating airplane: Convair 990.

Figure 4. Continued.

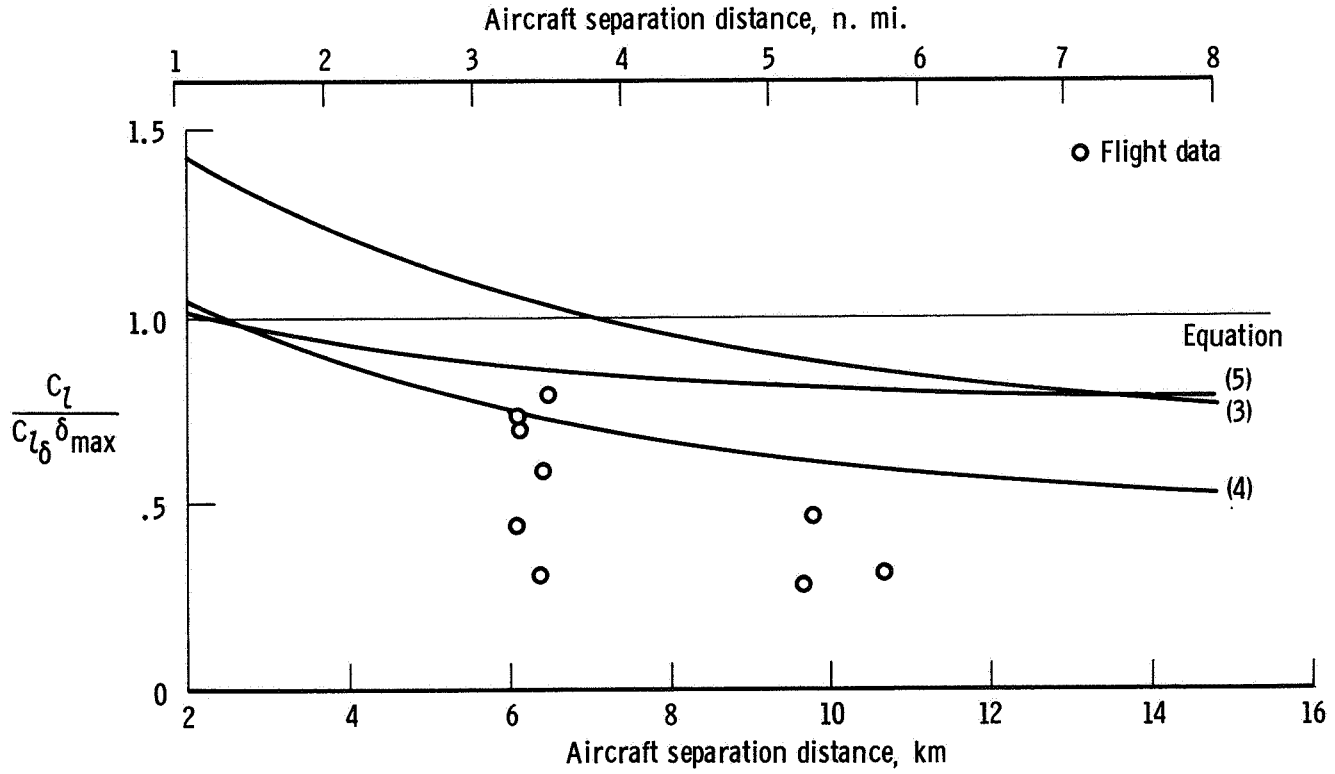

(e) Probe airplane: Learjet 23, V = 240 knots, $C_{l_\delta \delta_{max}} = 0.0472$; generating airplane: DC-9.

Figure 4. Continued.

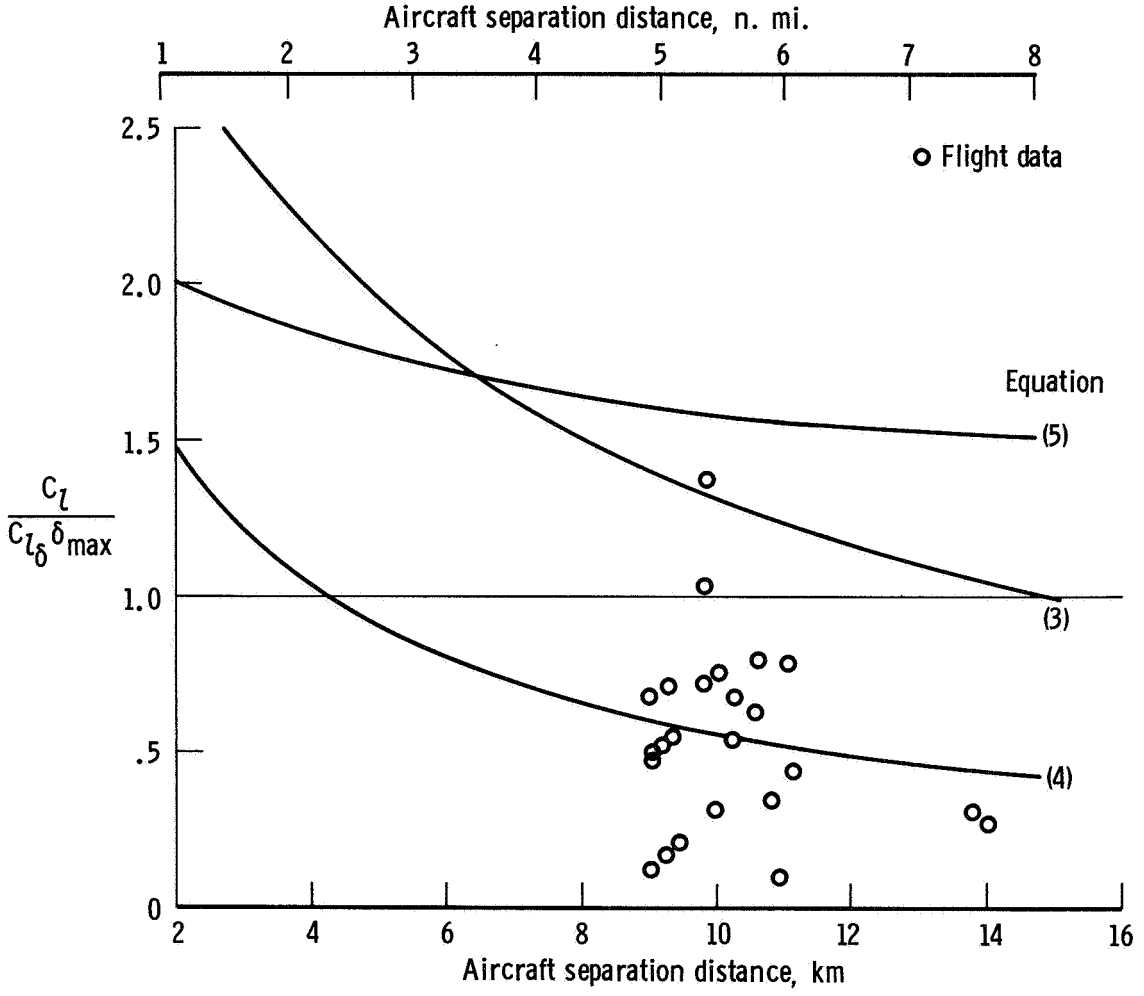

(f) Probe airplane: Cessna 210, V = 149 knots, $C_{l_\delta \delta_{max}} = 0.0560$; generating airplane: CV-990, V = 195 knots.

Figure 4. Concluded.

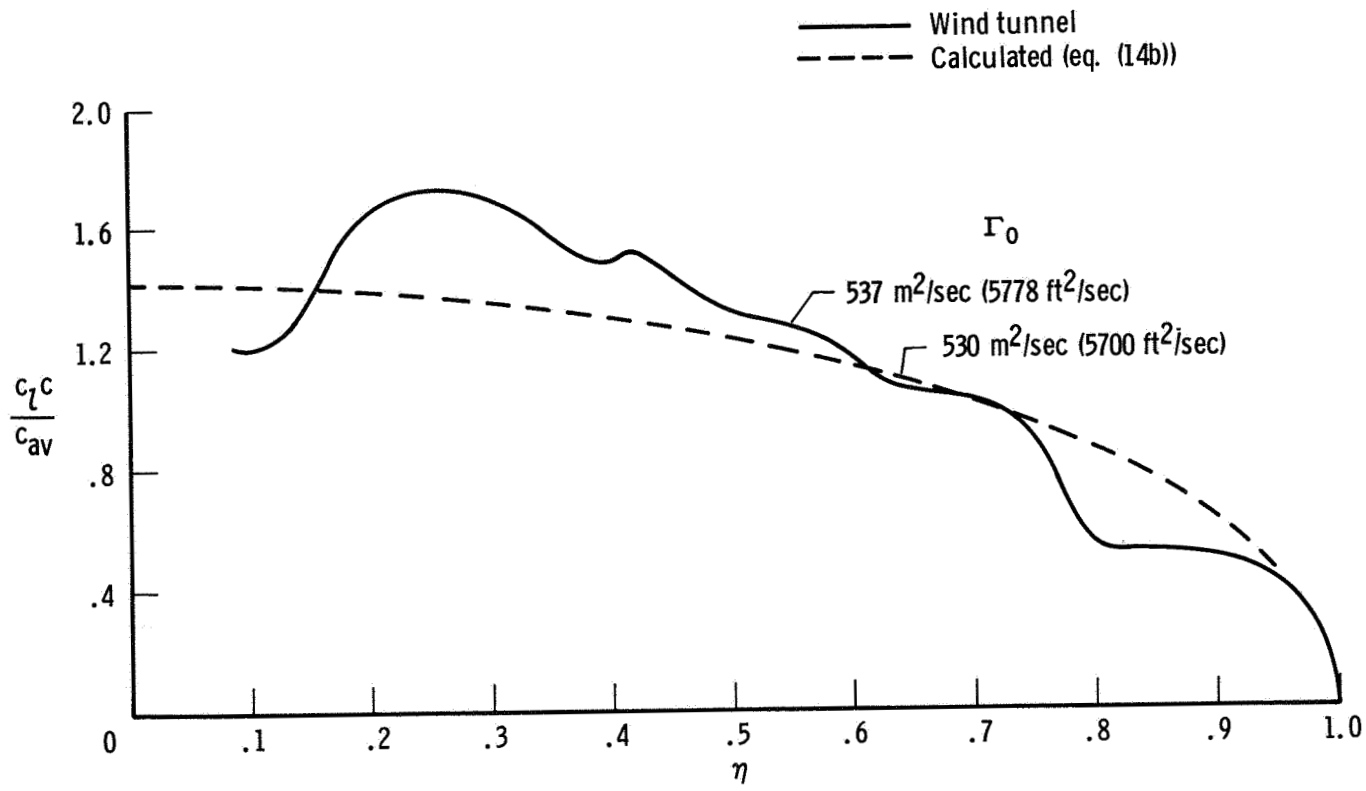

(a) Span load distribution.

Figure 5. Calculated and wind-tunnel values of span load and vorticity distribution for the C-5A airplane in the power approach configuration. $C_L = 1.11$; V = 169 knots.

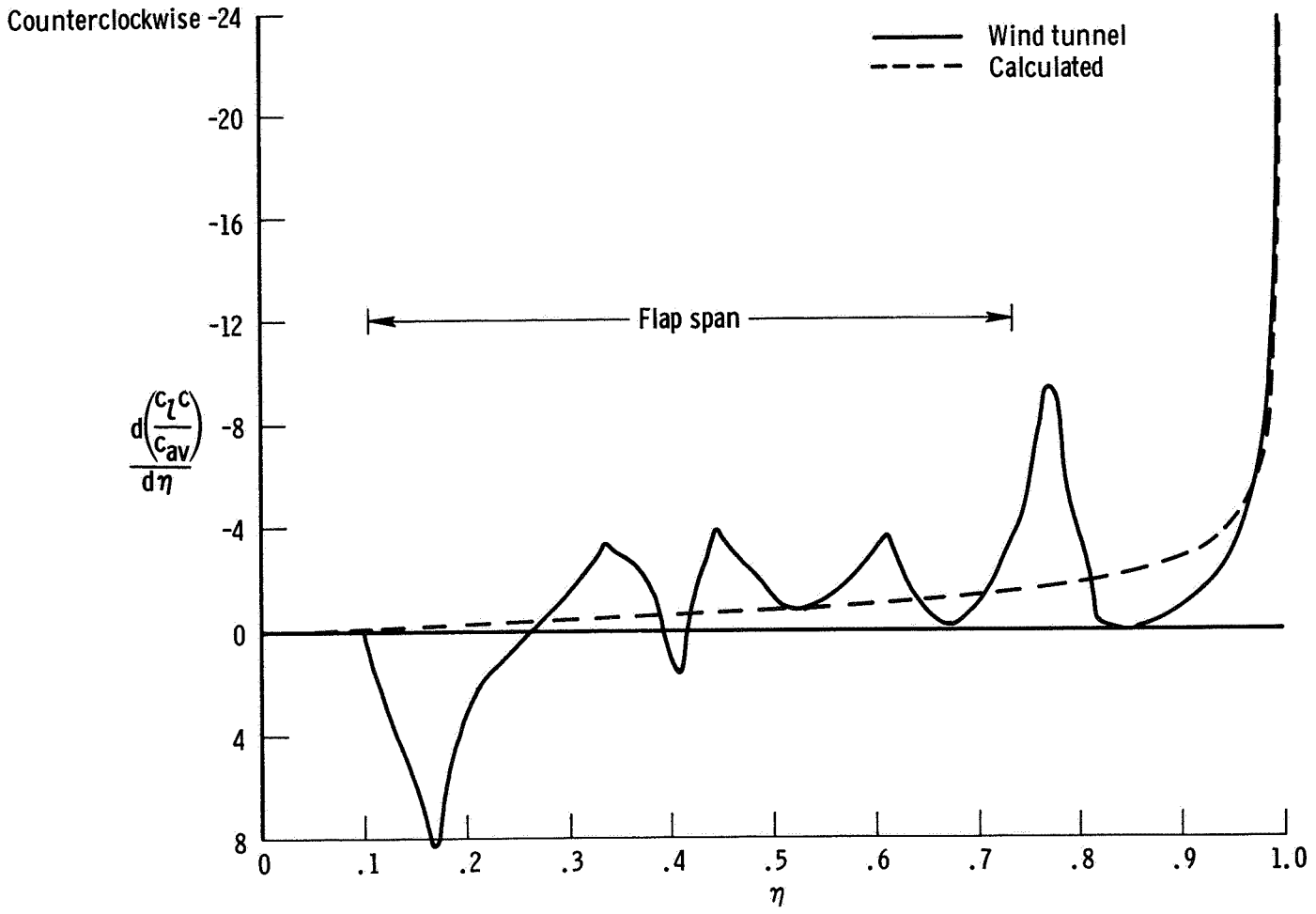

(b) Vorticity distribution.

Figure 5. Concluded.

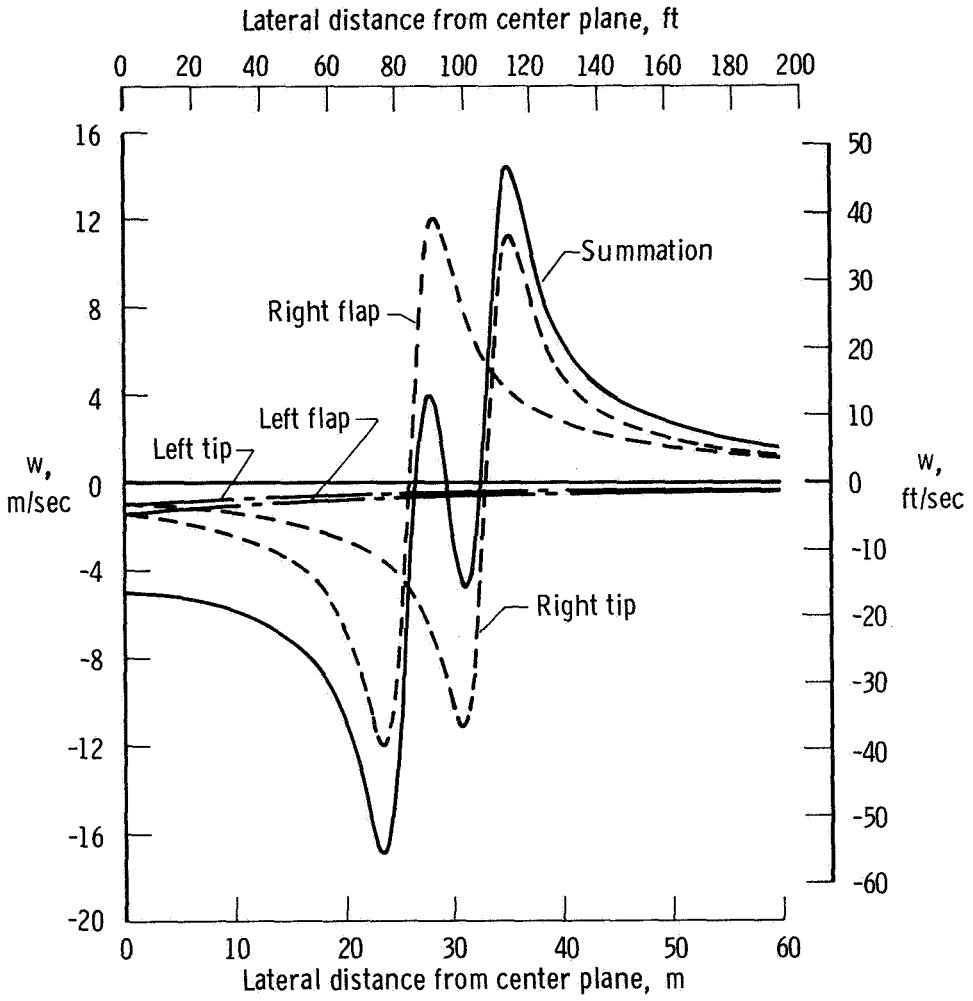

Figure 6. Net spanwise vertical-velocity distribution resulting from wingtip and flap outer-edge vortices as computed with equation (3). C-5A airplane; power approach configuration; V = 169 knots; separation distance = 1.85 km (1.0 n. mi.).

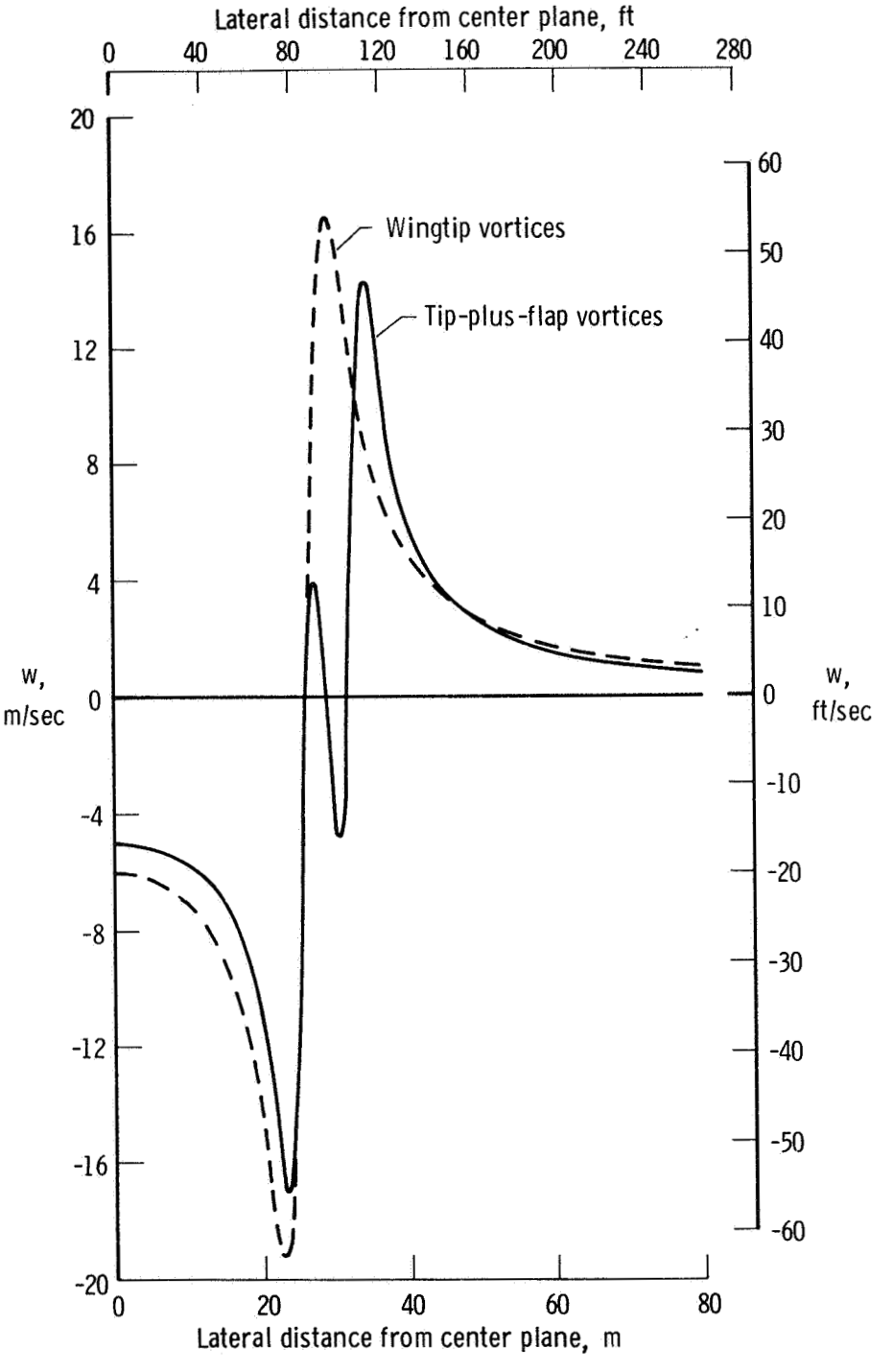

(a) Separation distance = 1.85 km (1.0 n. mi.).

Figure 7. Calculated (eq. (3)) wingtip and wingtip-plus-flap vortex systems as a function of semispan length for the C-5A airplane in the power approach configuration. V = 169 knots.

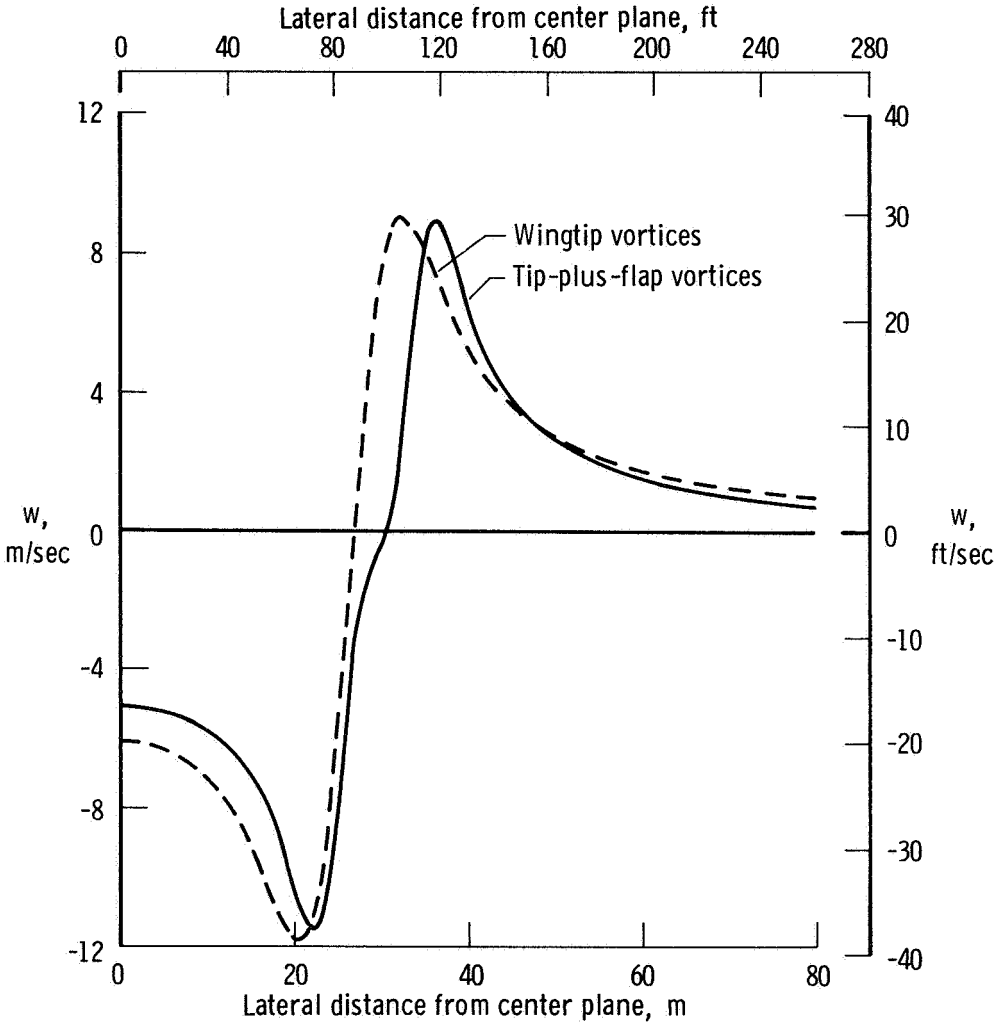

(b) Separation distance = 5.56 km (3.0 n. mi.).

Figure 7. Continued.

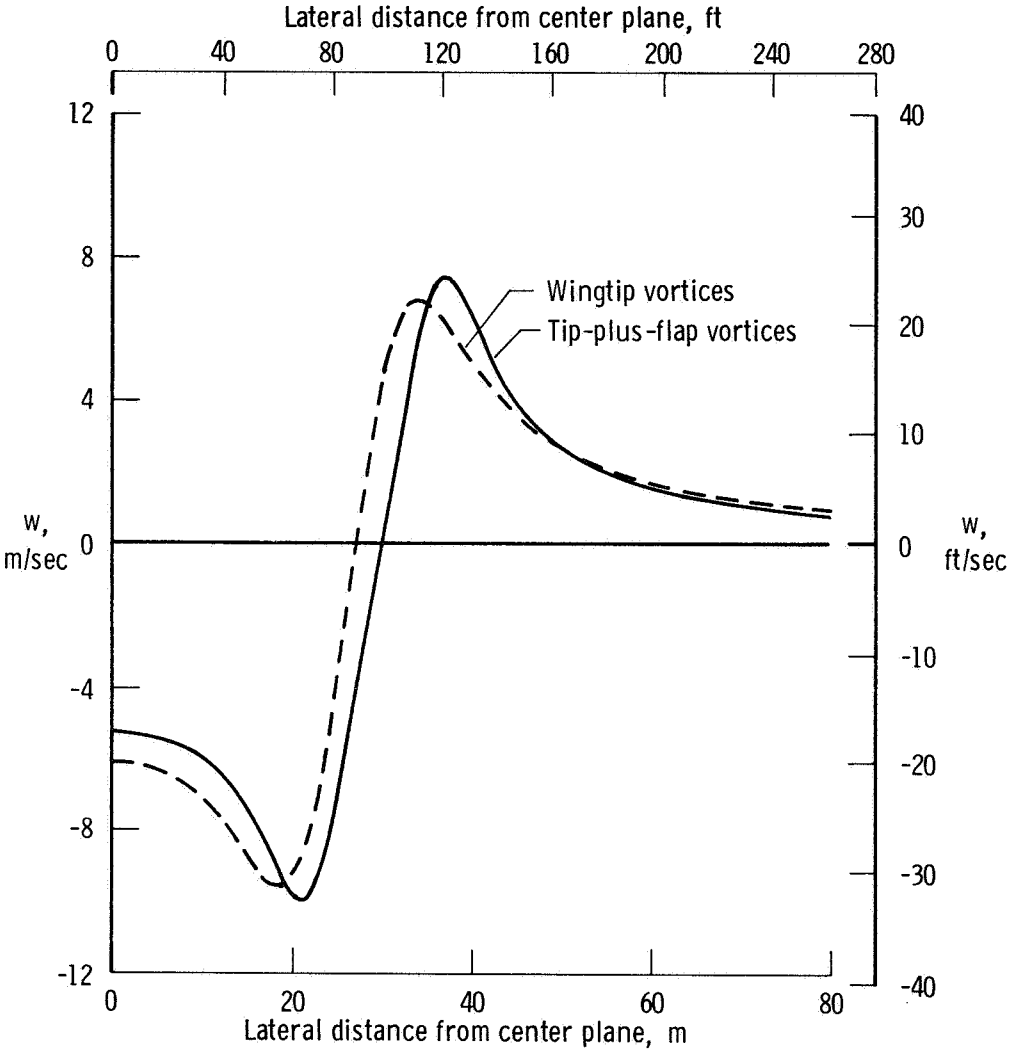

(c) Separation distance = 9.26 km (5.0 n. mi.).

Figure 7. Concluded.

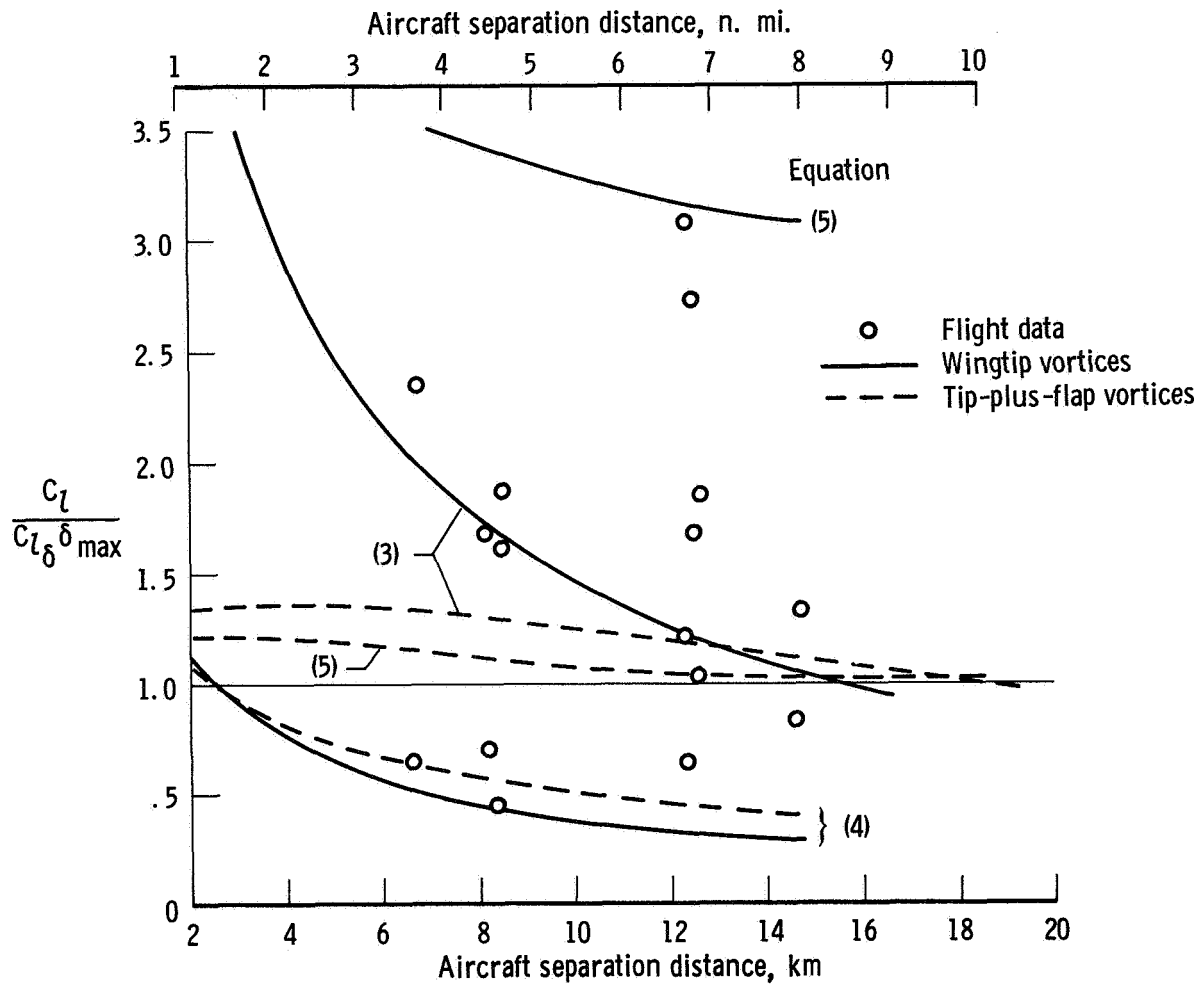

Figure 8. Comparison of calculated and flight-test rolling-moment ratios for the Learjet 23 (probe airplane) and C-5A (generating airplane) in the power approach configuration. V = 169 knots; $C_{l_\delta}\delta_{max} = 0.0463$.

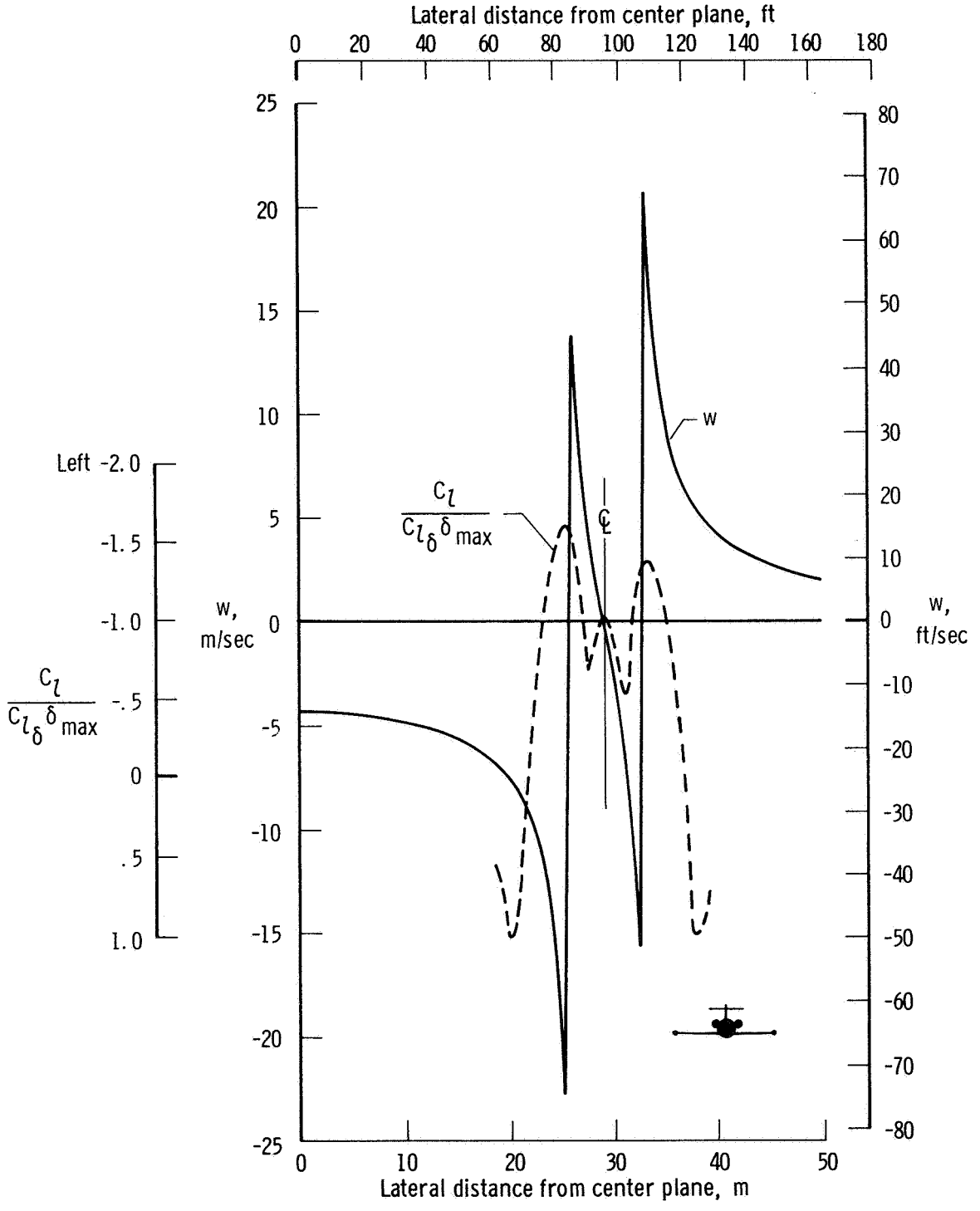

Figure 9. Change in rolling-moment ratio with lateral displacement of probe airplane across wake cross section as computed with equation (5). Probe airplane: Learjet 23; generating airplane: C-5A; power approach configuration; V = 169 knots; separation distance = 13.0 km (7.0 n. mi.).

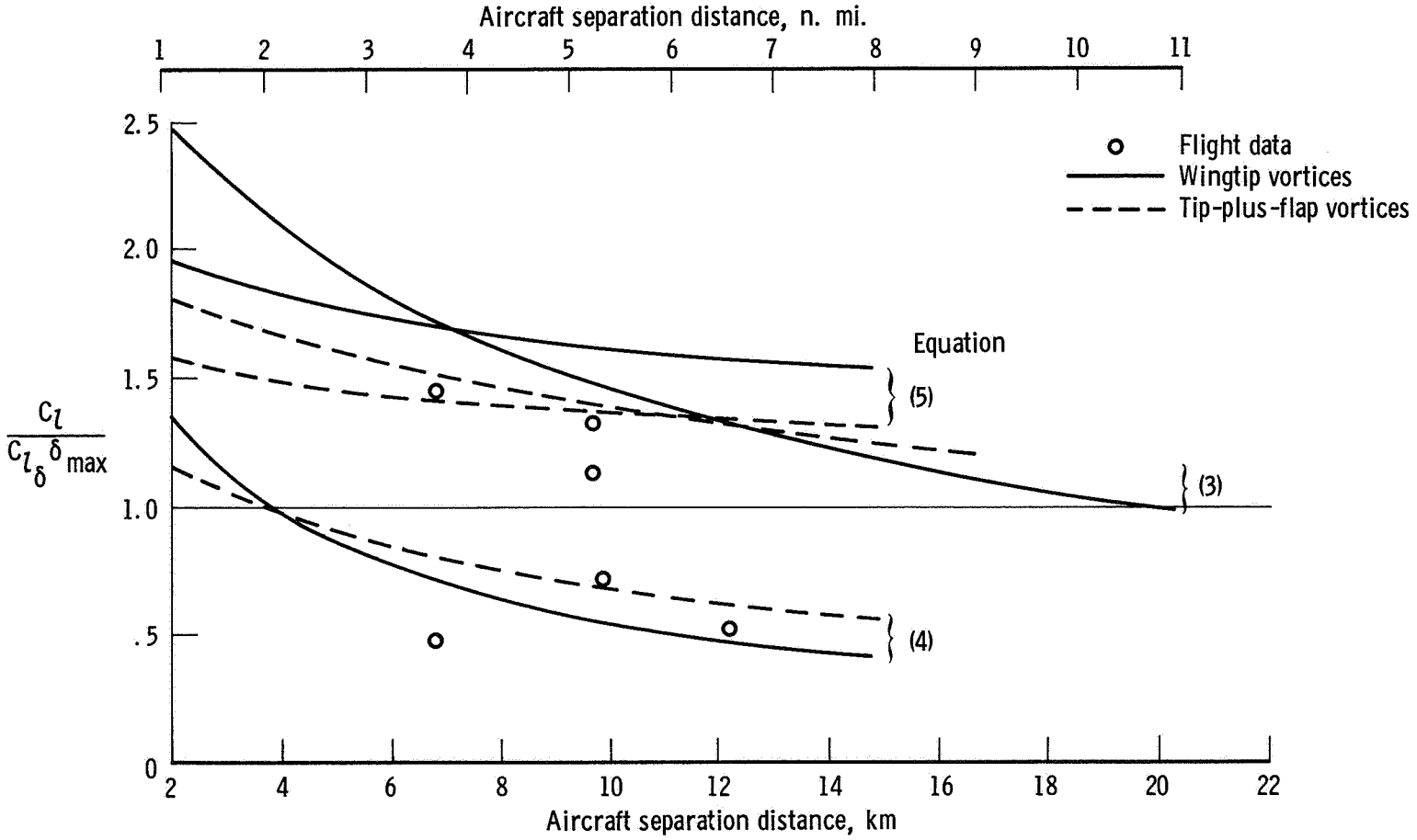

(a) Probe airplane: DC-9, landing configuration, V = 181 knots, $C_{l_\delta \delta_{max}} = 0.0650$; generating airplane: C-5A.

Figure 10. Comparison of calculated and flight-test rolling-moment ratios for several combinations of probe and generating aircraft. Wing flaps extended configuration.

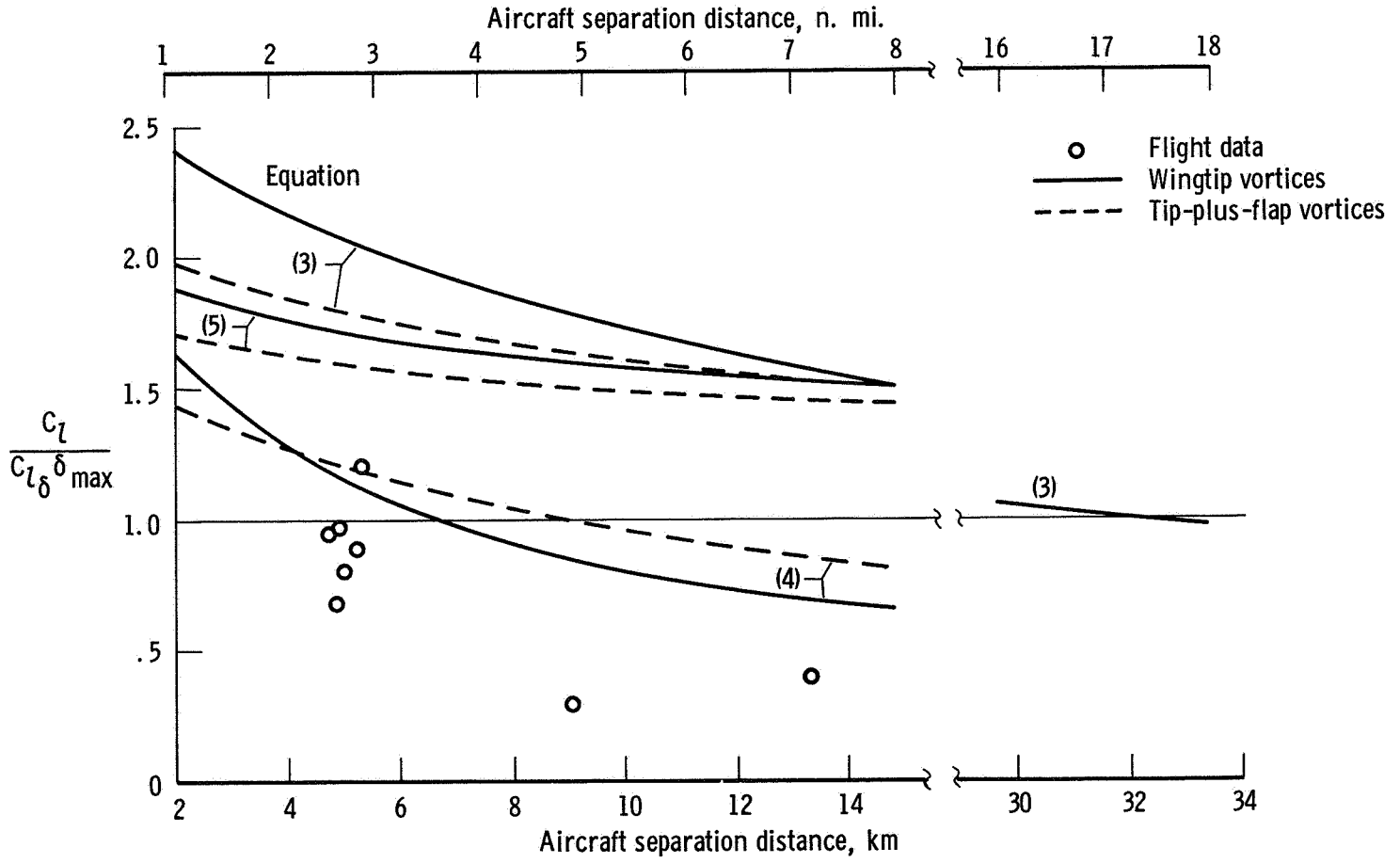

(b) Probe airplane: Convair 990, power approach configuration, V = 181 knots, $C_{l_\delta \delta_{max}} = 0.0589$; generating airplane: C-5A.

Figure 10. Continued.

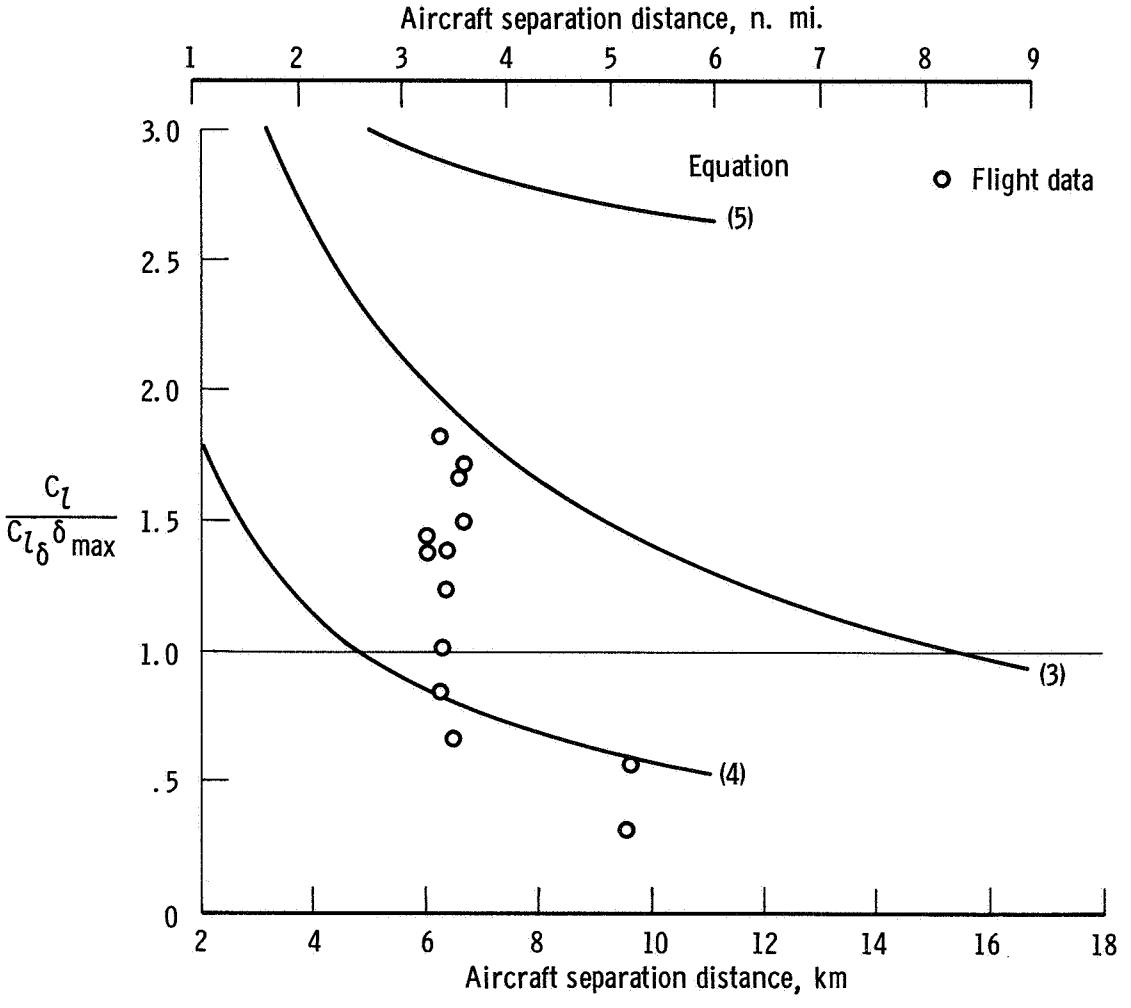

(c) Probe airplane: Learjet 23, landing configuration, V = 181 knots, $C_{l_\delta \delta_{max}} = 0.0455$; generating airplane: Convair 990.

Figure 10. Continued.

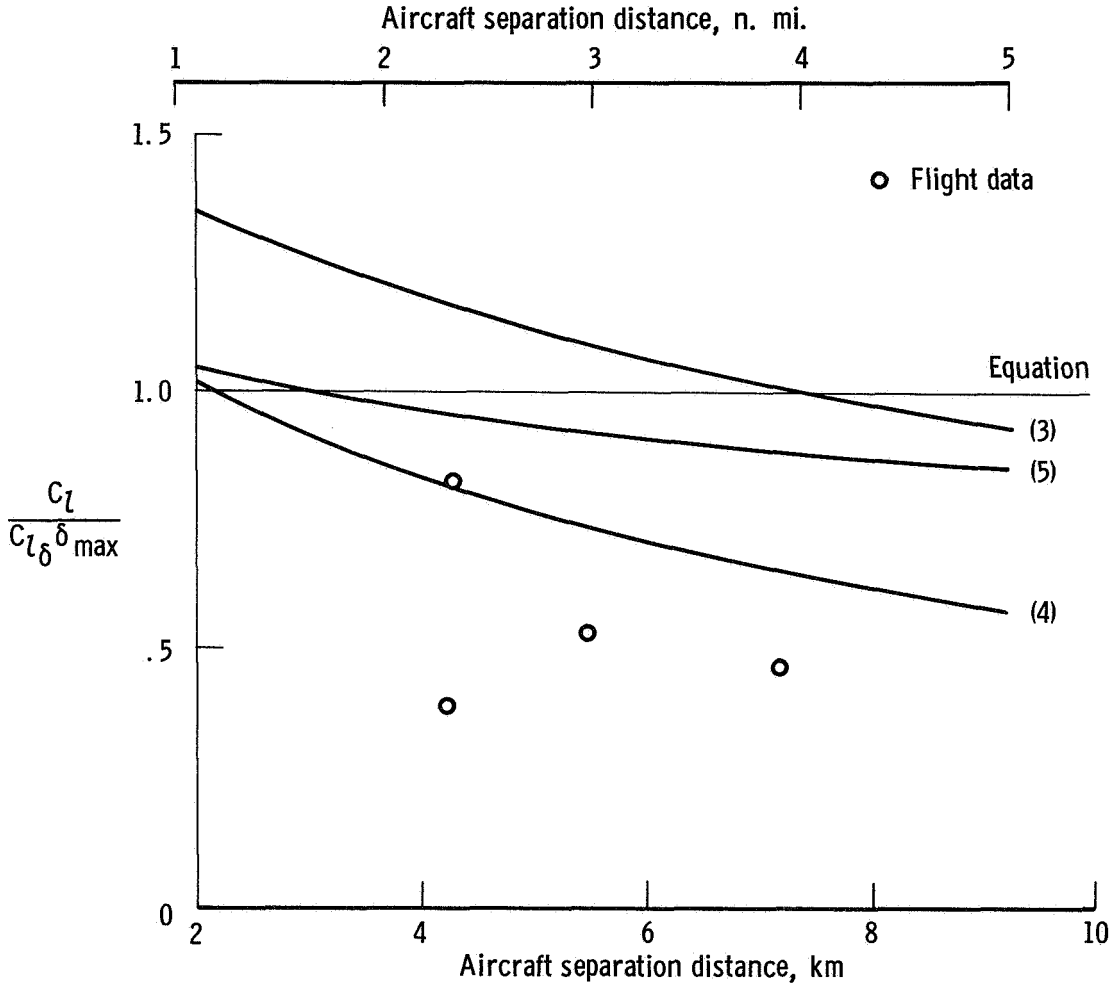

(d) Probe airplane: DC-9, landing configuration, V = 181 knots, $C_{l_\delta}\delta_{max} = 0.0850$; generating airplane: Convair 990.

Figure 10. Concluded.

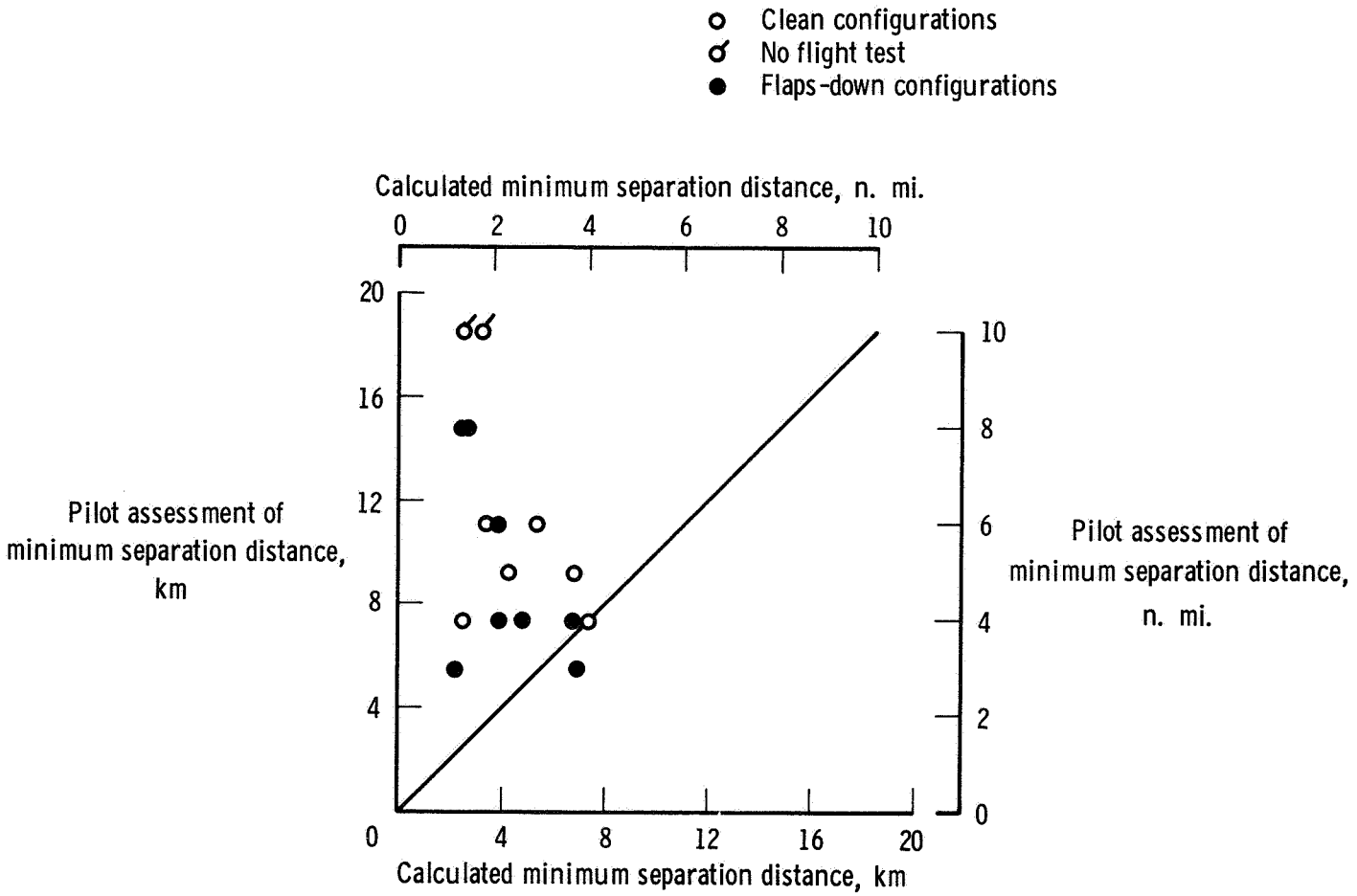

(a) Wetmore and Reeder expression (eq. (4)).

Figure 11. Comparison of calculated minimum separation distance with the pilot assessment.

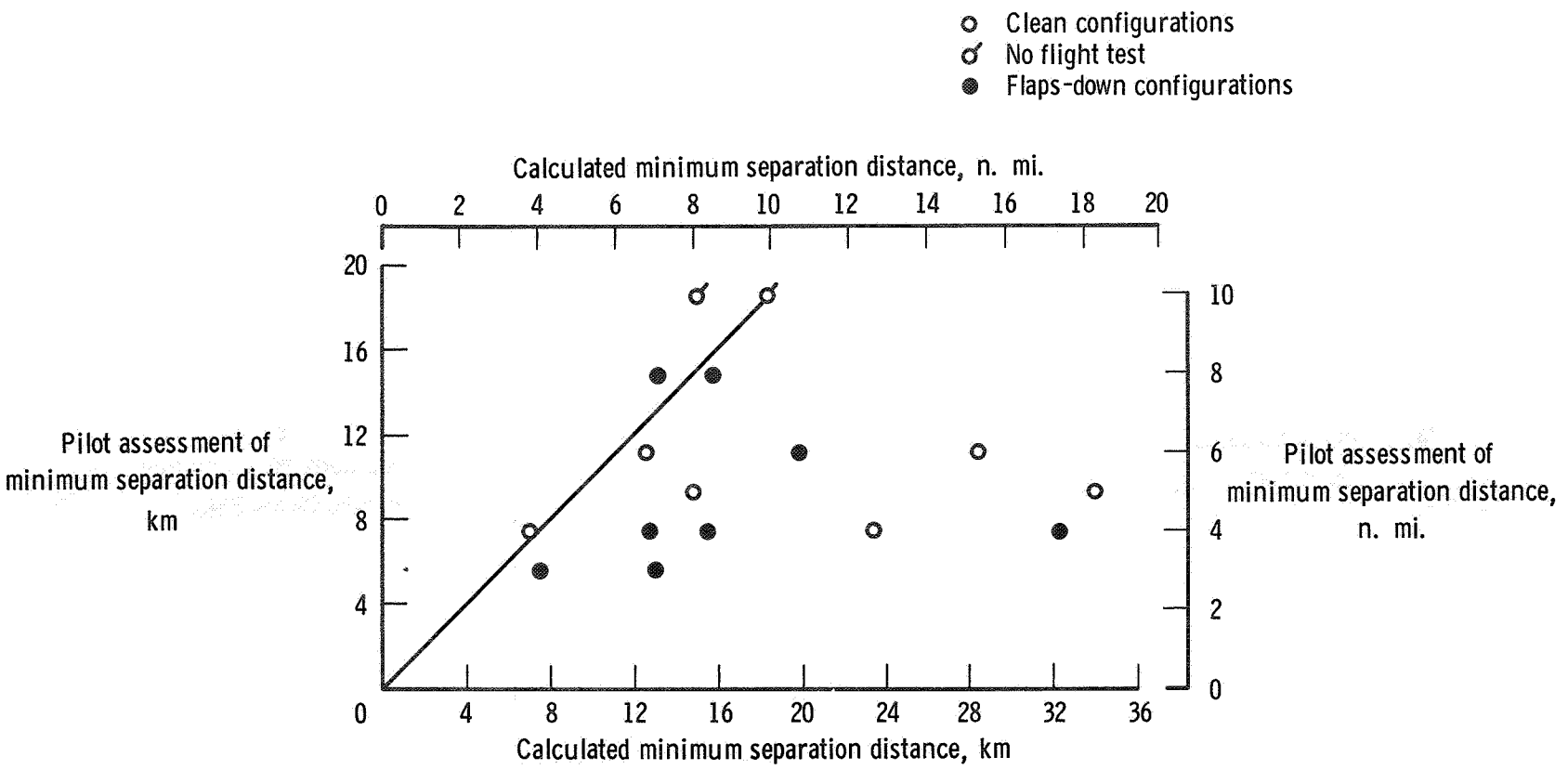

(b) Kerr, Rose, and Dee expression (eq. (3)).

Figure 11. Concluded.

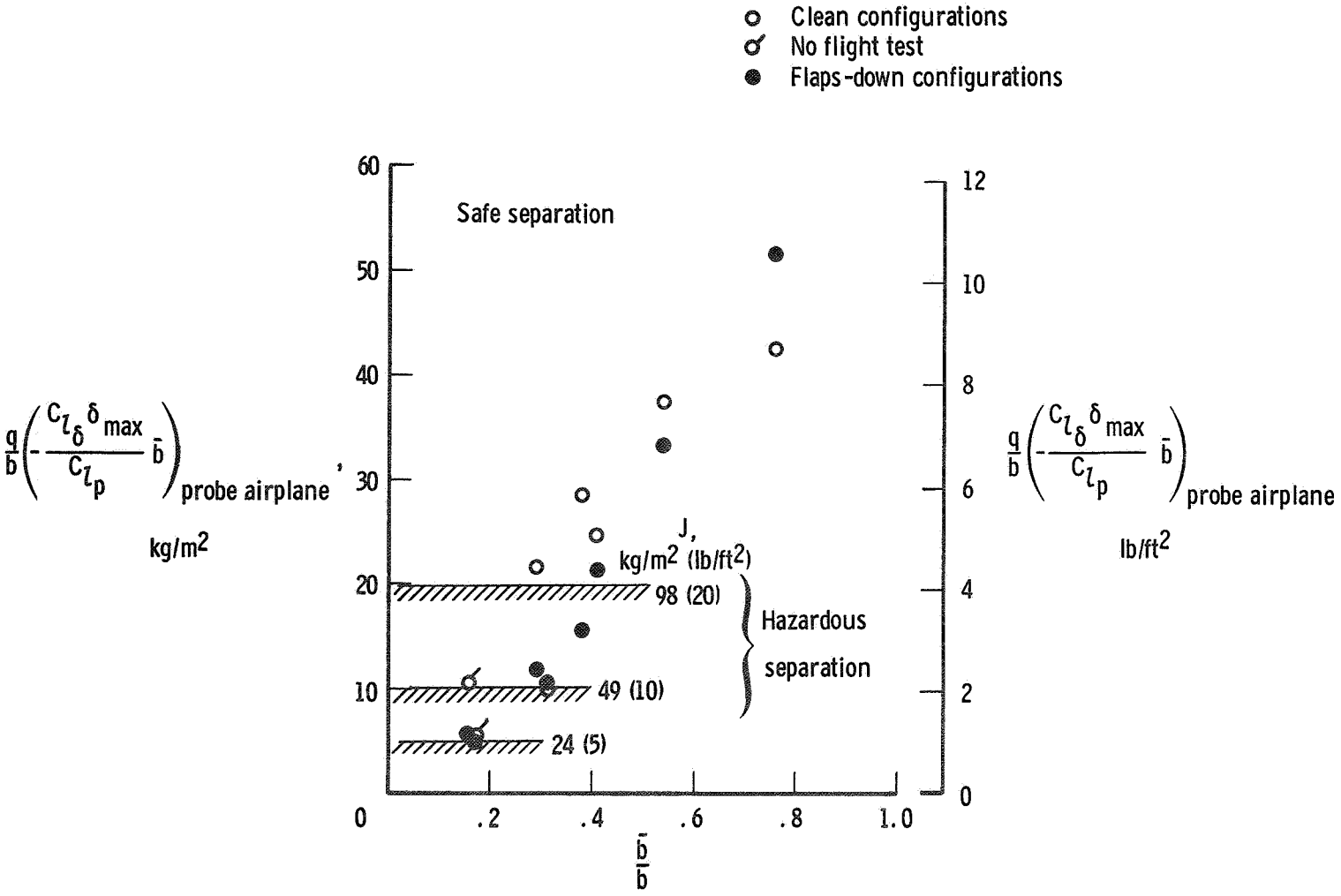

Figure 12. Variation of the vortex hazard expression in terms of the wingspan ratios of the probe and generating airplanes.

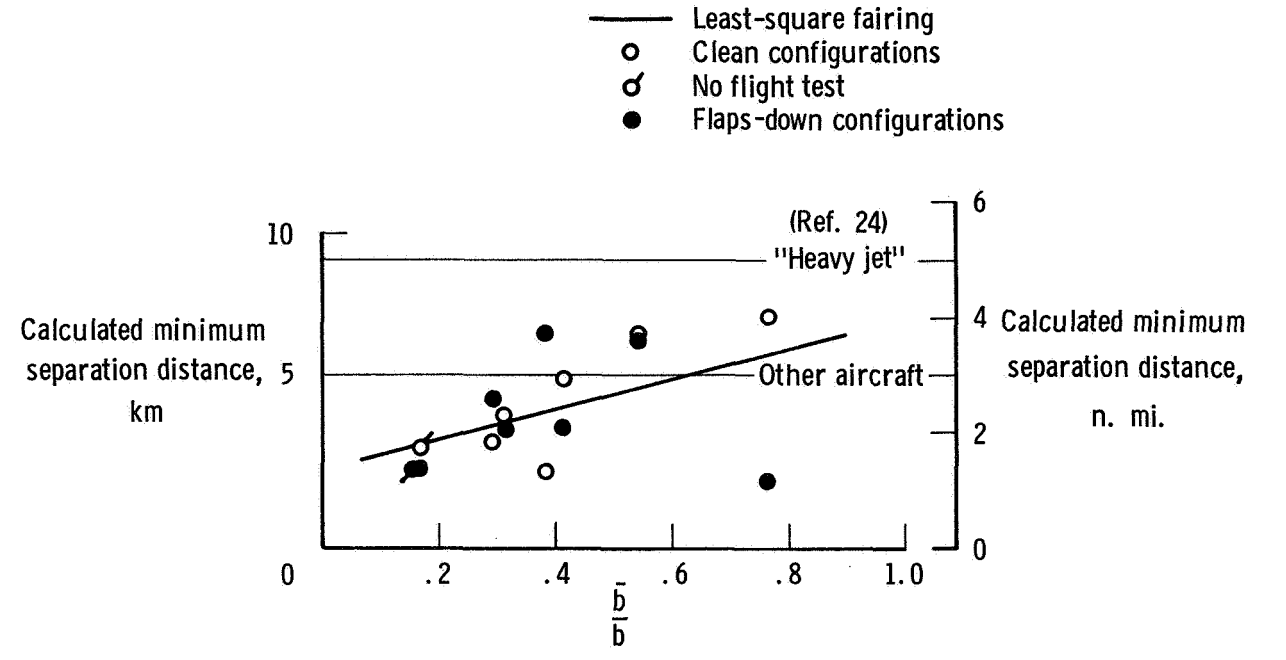

(a) Wetmore and Reeder expression (eq. (4)).

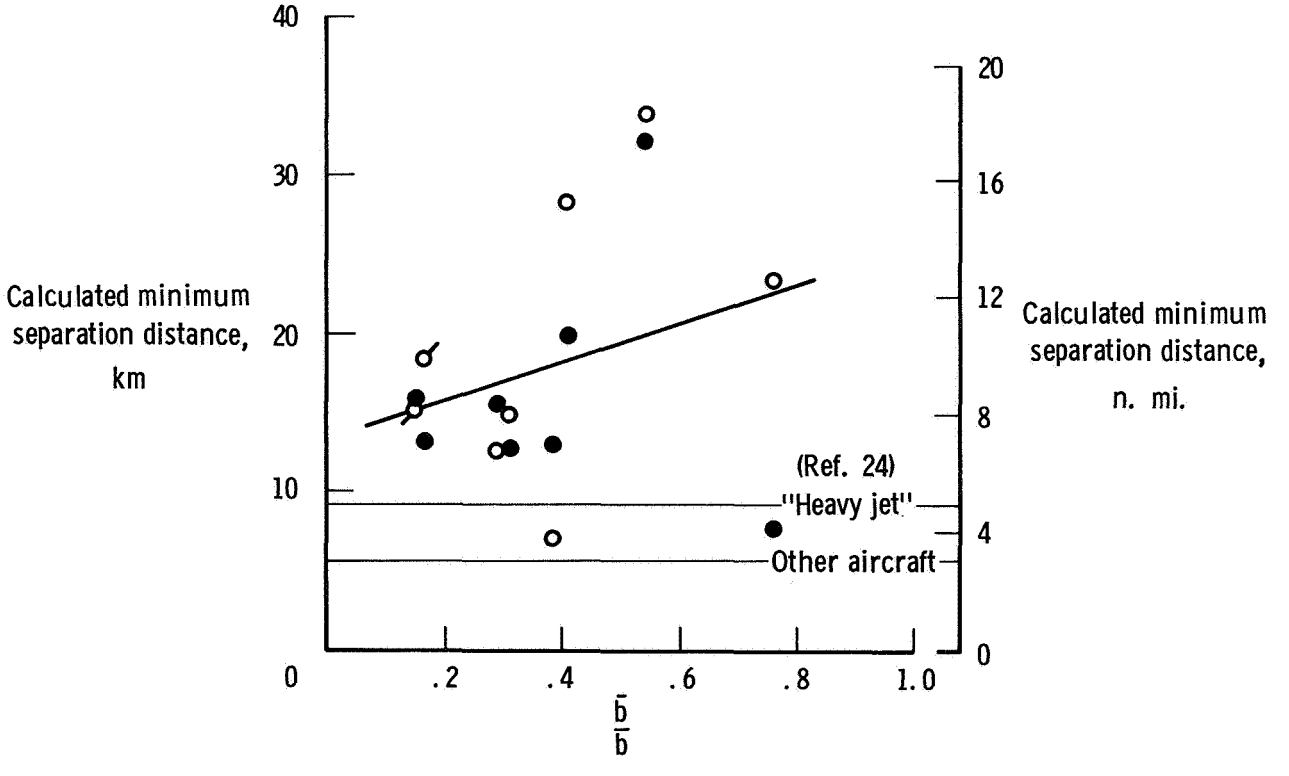

(b) Kerr, Rose, and Dee expression (eq. (3)).

Figure 13. Variation of calculated minimum separation distances in terms of the wing-span ratio of the probe and generating aircraft.

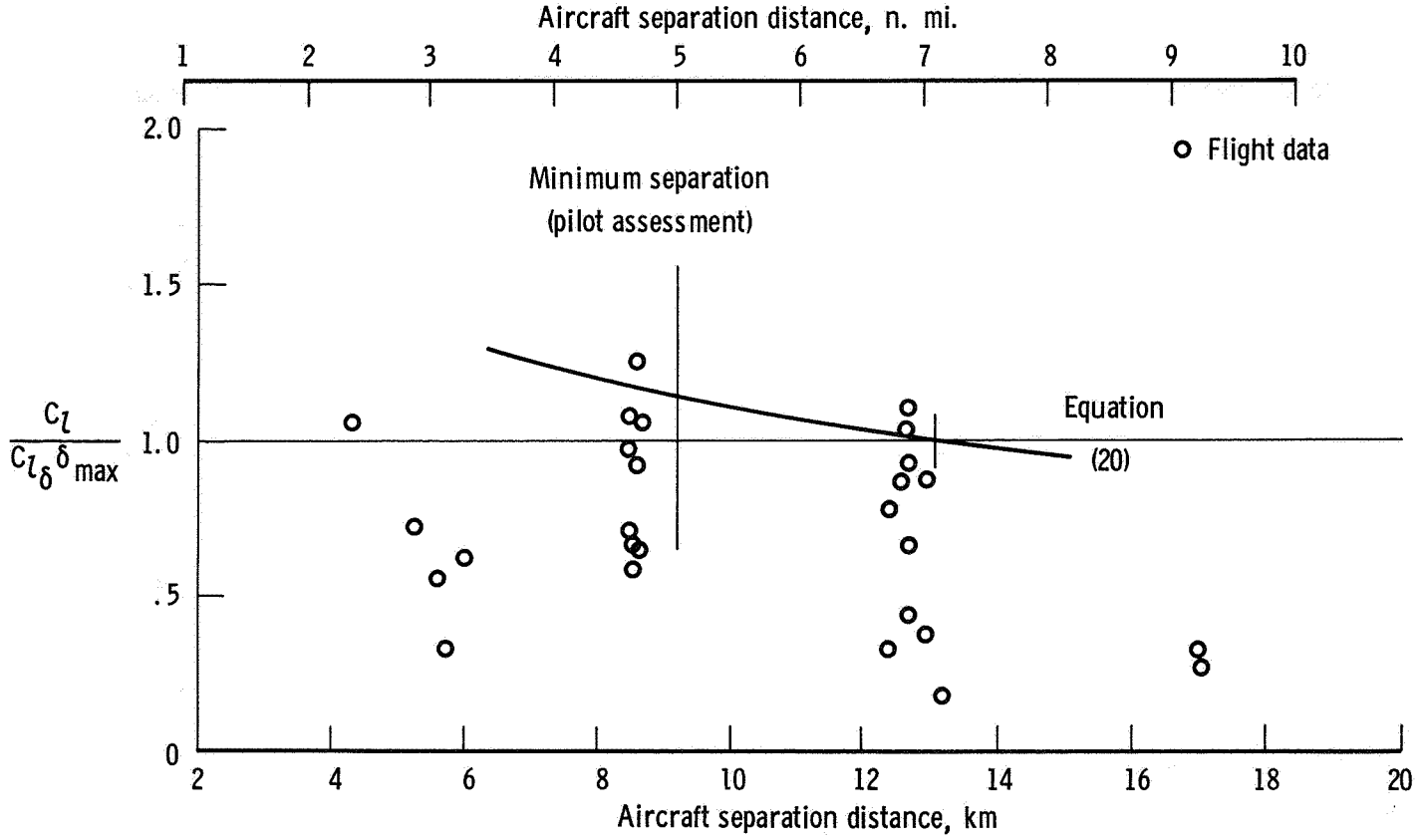

(a) Probe airplane: Convair 990, clean configuration, V = 229 knots; generating airplane: C-5A.

Figure 14. Summary of calculated and flight-test rolling-moment ratios and pilot assessment of the minimum separation distance for various combinations of probe and generating aircraft.

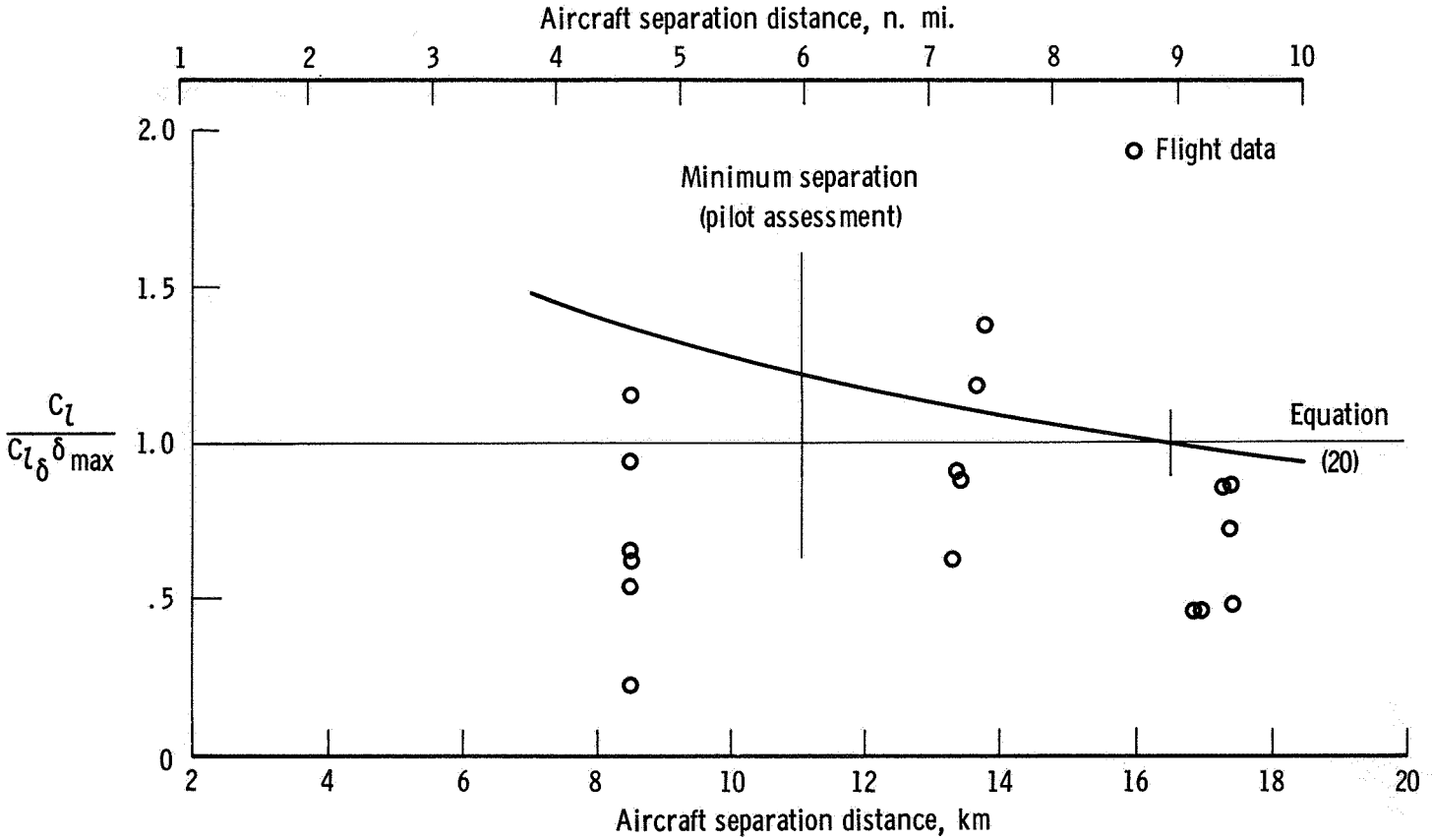

(b) Probe airplane: DC-9, clean configuration, V = 229 knots; generating airplane: C-5A.

Figure 14. Continued.

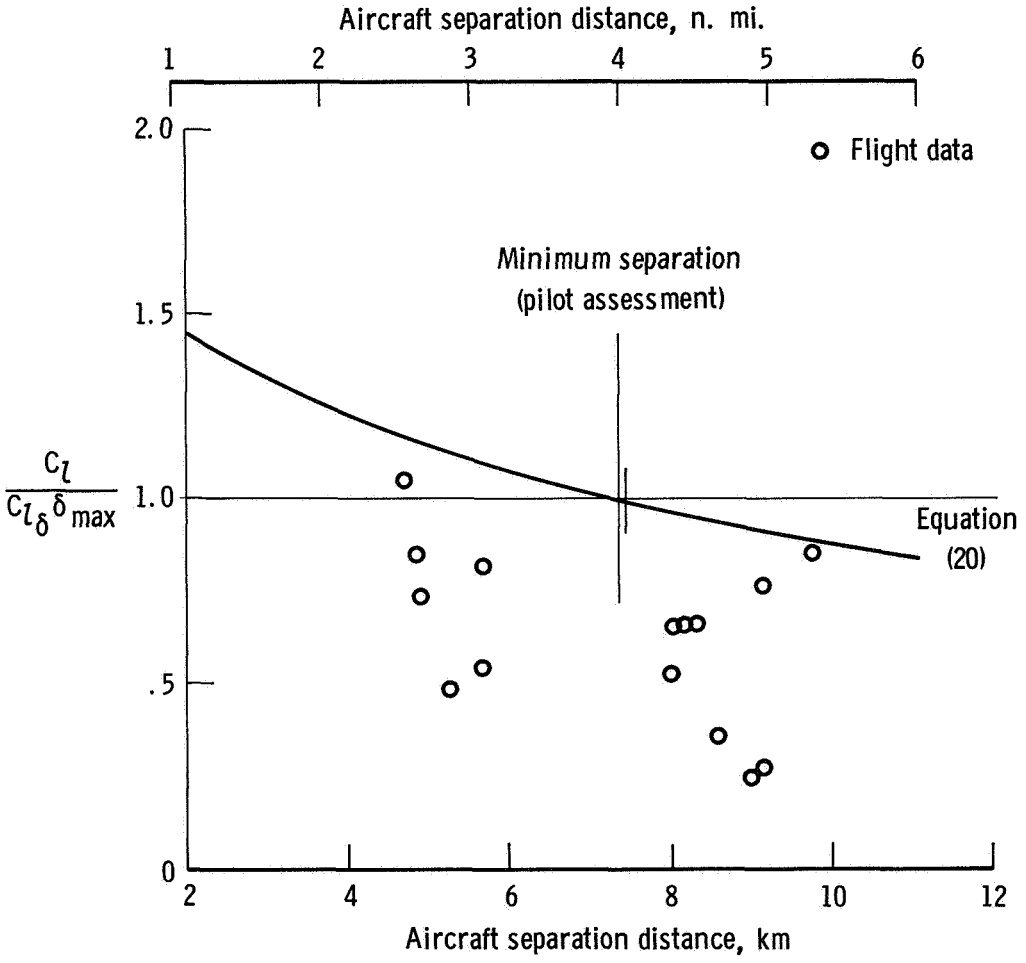

(c) Probe airplane: DC-9, clean configuration, V = 216 knots; generating airplane: Convair 990.

Figure 14. Continued.

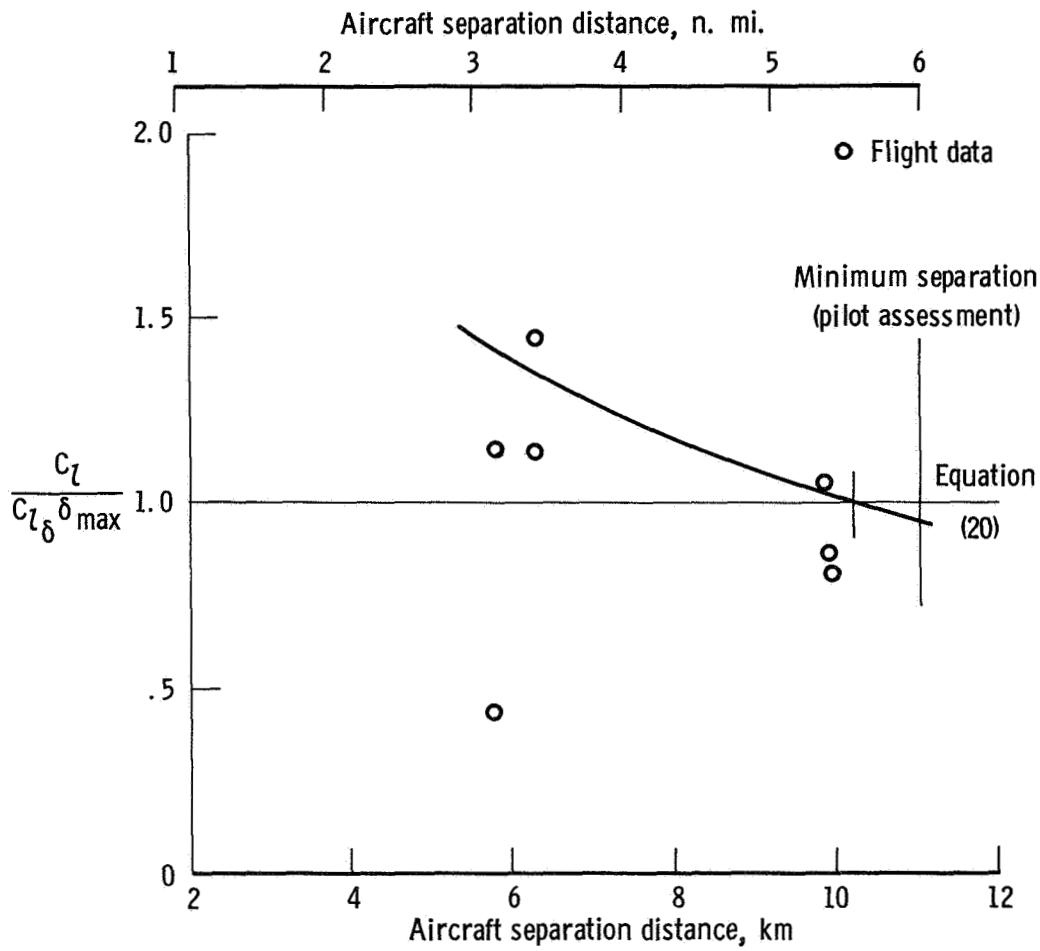

(d) Probe airplane: Learjet 23, clean configuration, V = 240 knots; generating airplane: Convair 990.

Figure 14. Continued.

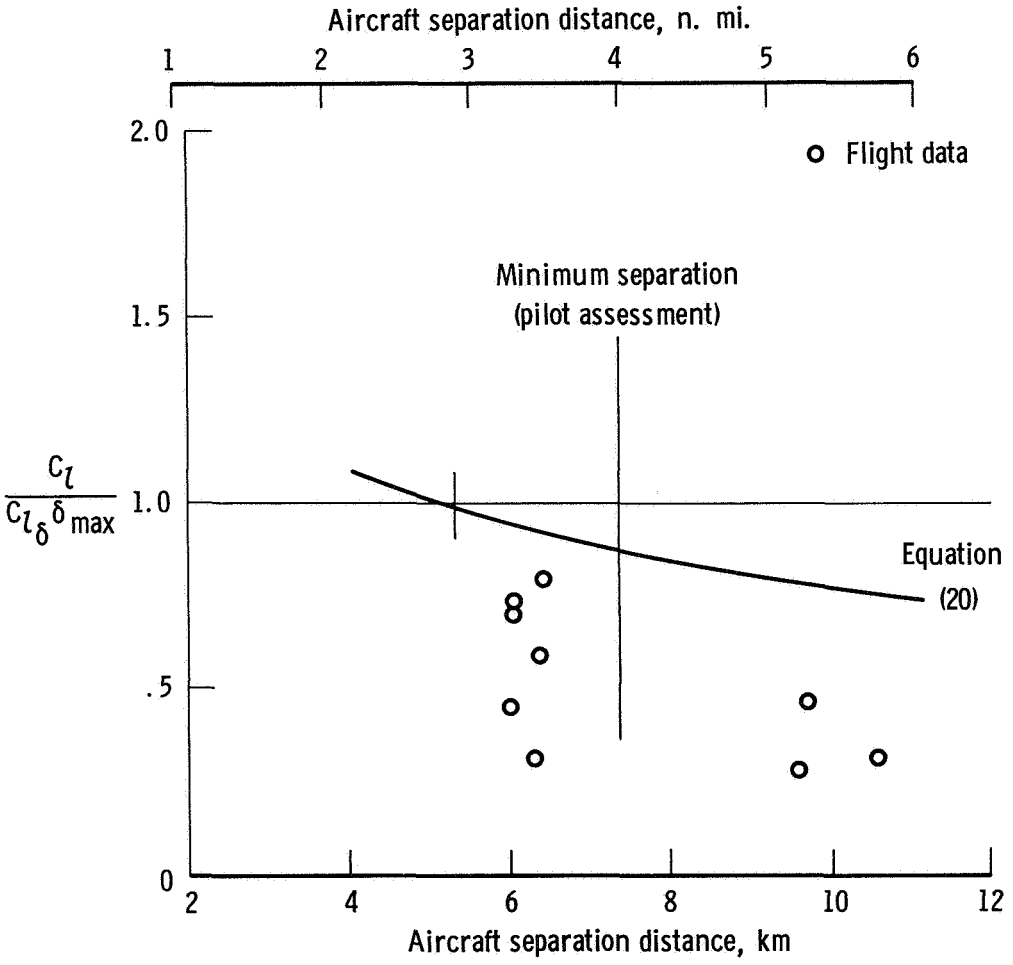

(e) Probe airplane: Learjet 23, clean configuration, V = 240 knots; generating airplane: DC-9.

Figure 14. Continued.

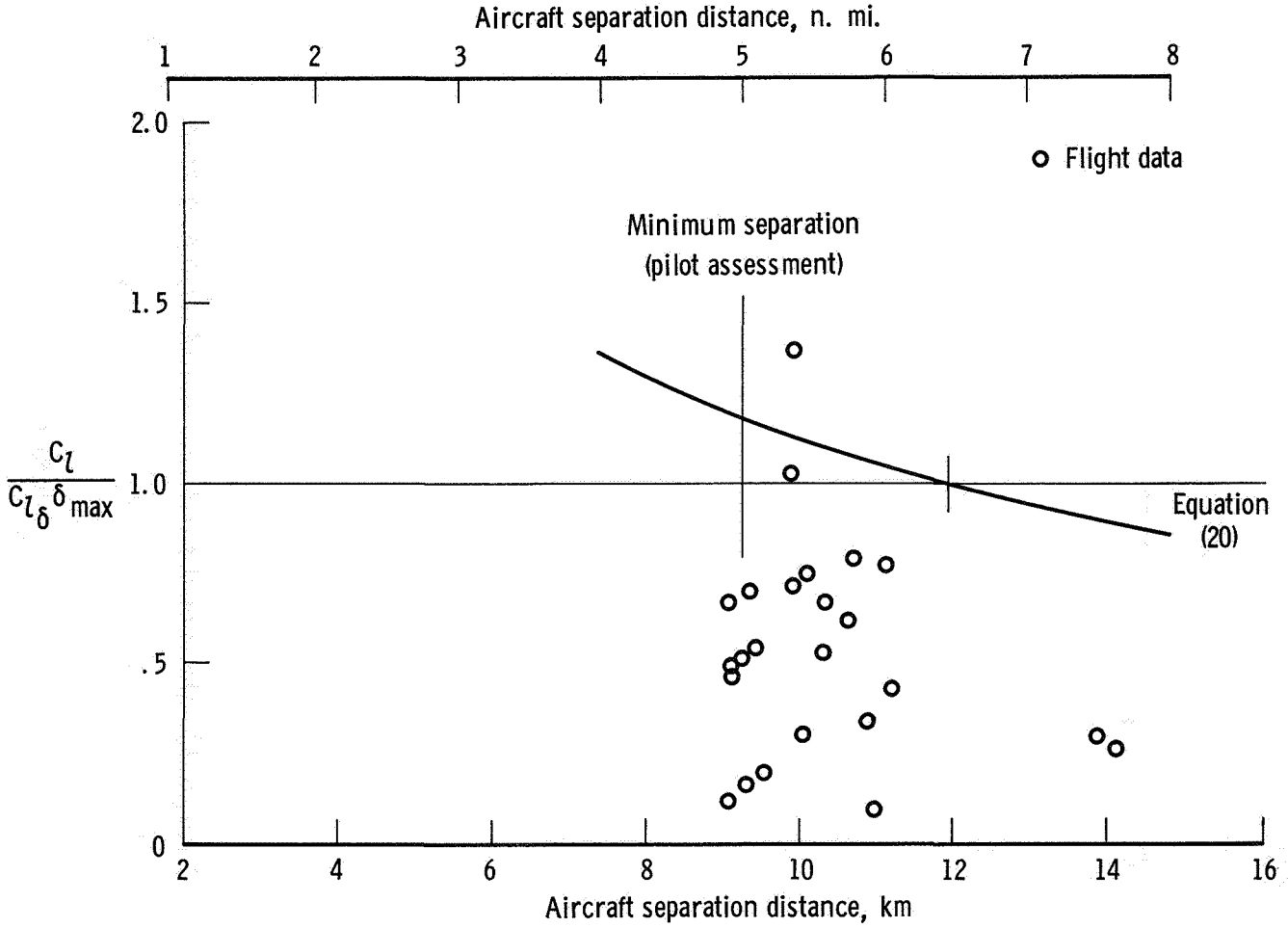

(f) Probe airplane: Cessna 210, clean configuration, V = 149 knots; generating airplane: Convair 990, V = 195 knots.

Figure 14. Continued.

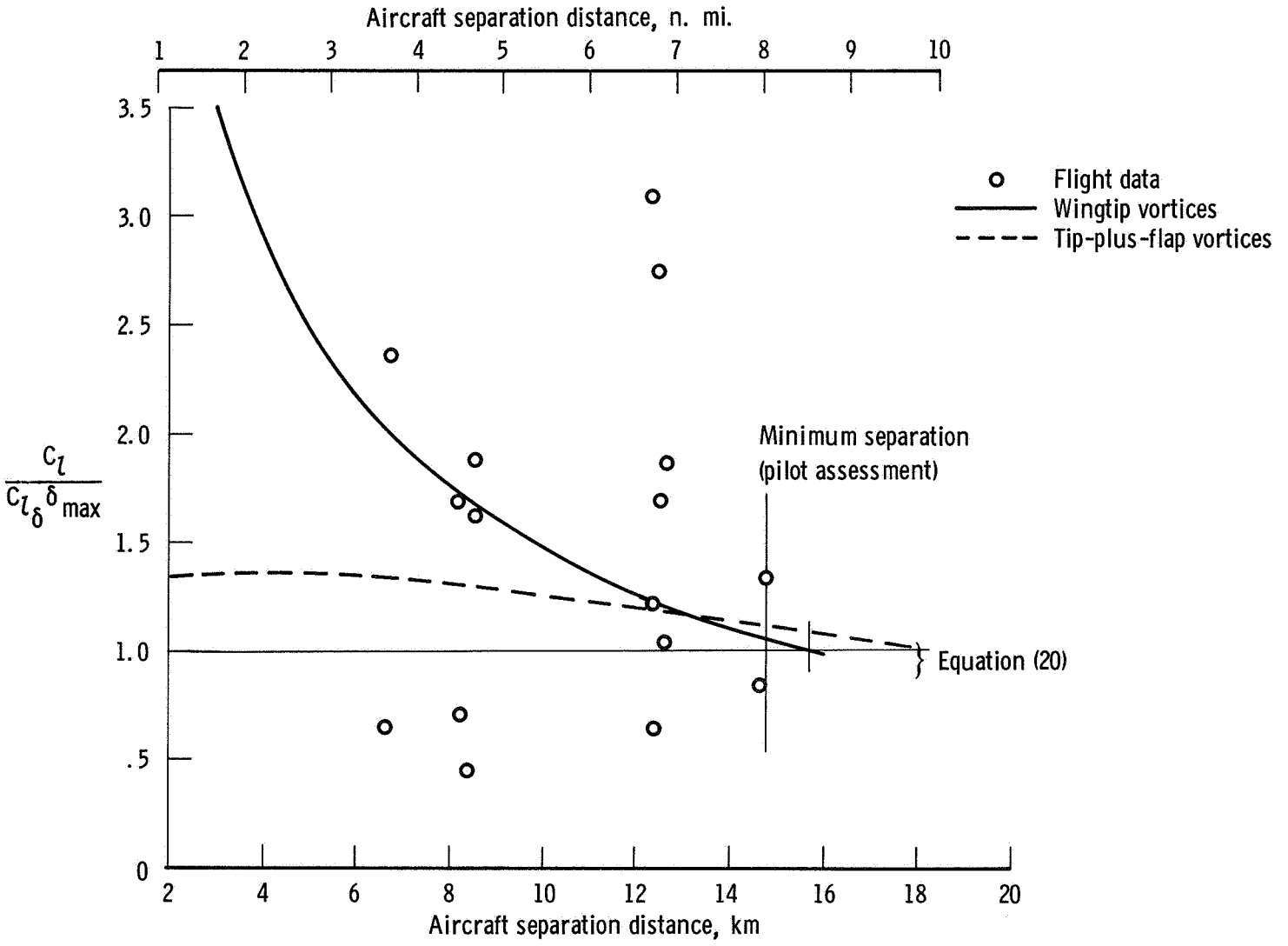

(g) Probe airplane: Learjet 23, power approach configuration, V = 169 knots; generating airplane: C-5A.

Figure 14. Continued.

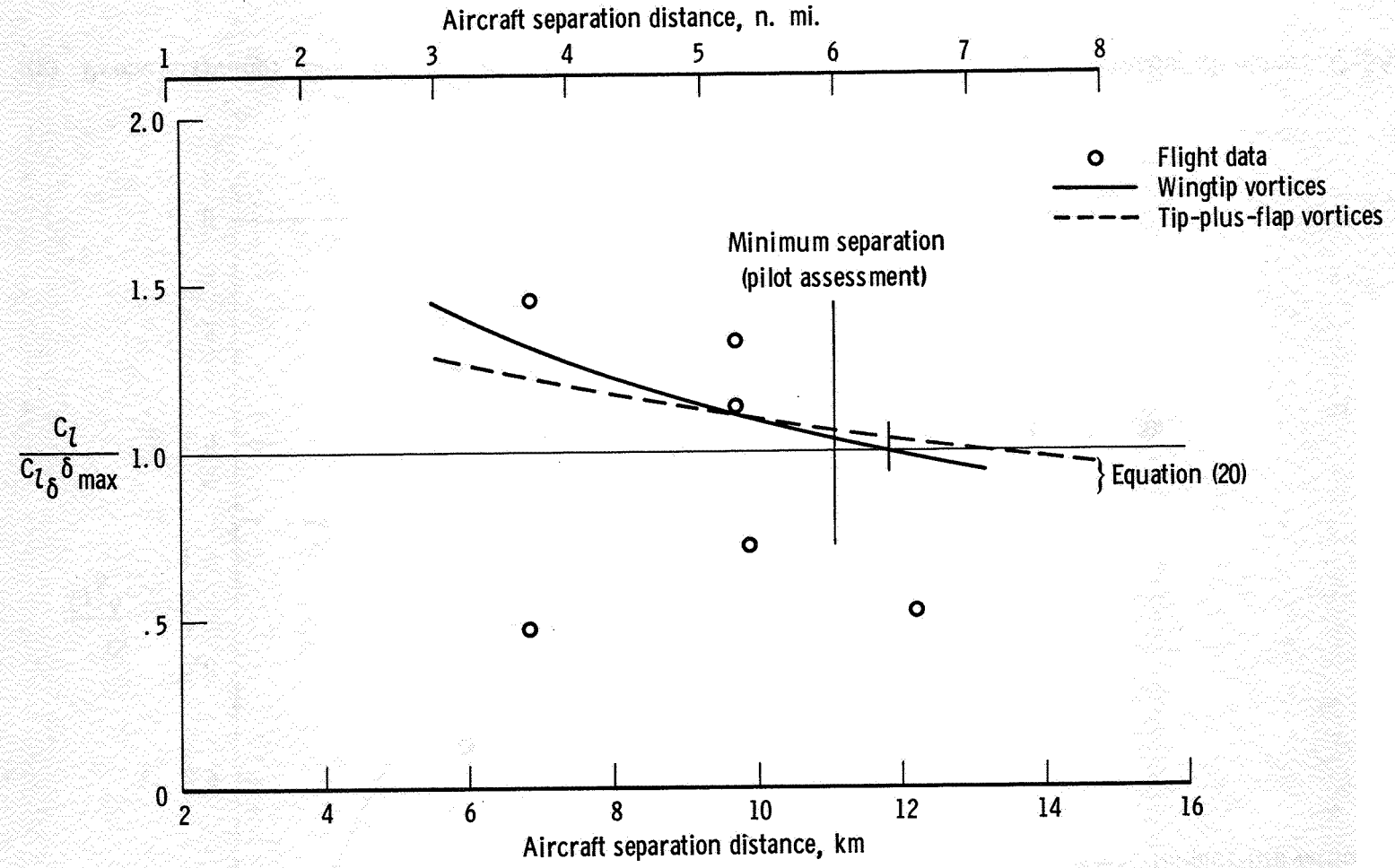

(h) Probe airplane: DC-9, landing configuration, V = 181 knots; generating airplane: C-5A.

Figure 14. Continued.

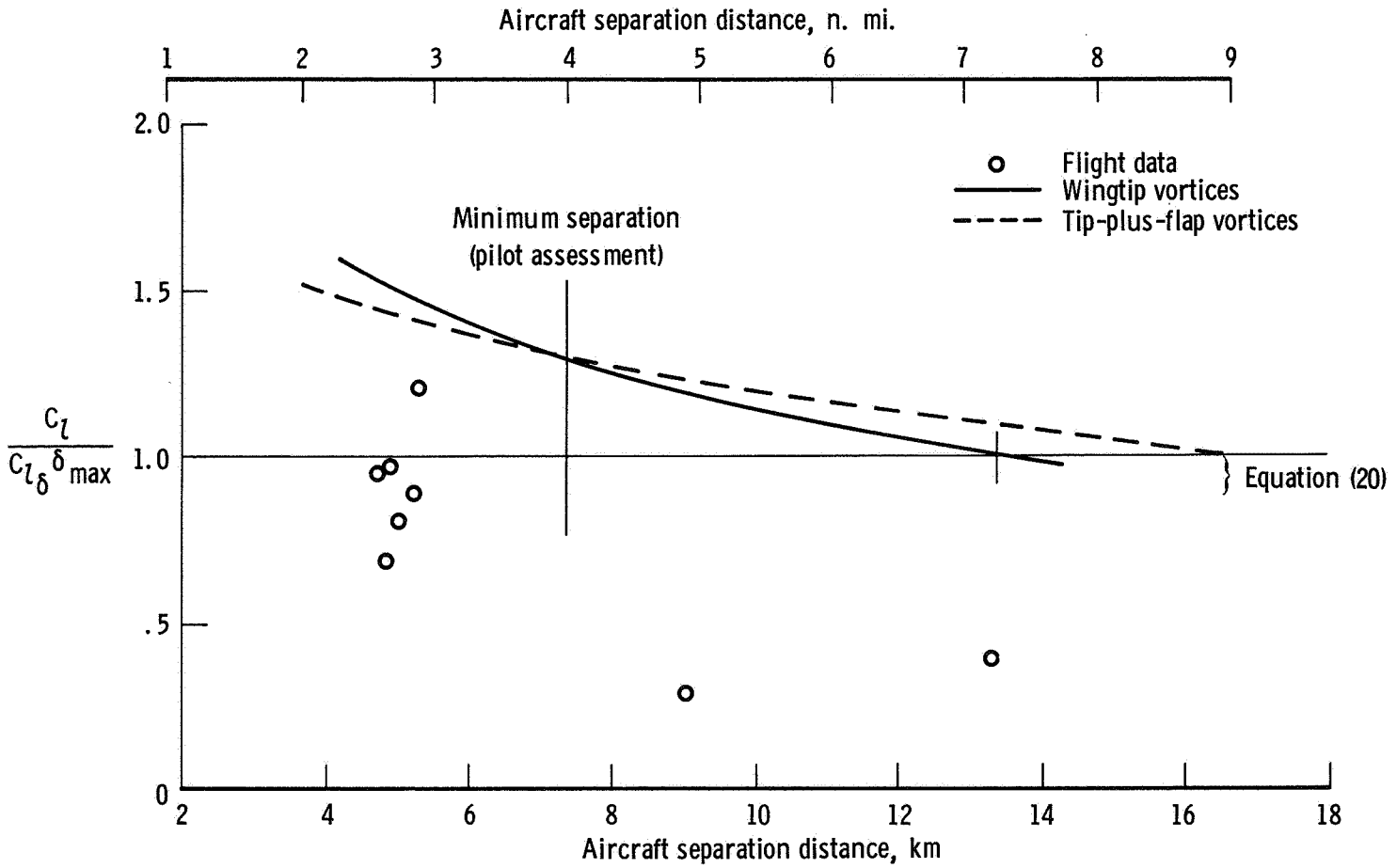

(i) Probe airplane: Convair 990, power approach configuration, V = 181 knots; generating airplane: C-5A.

Figure 14. Continued.

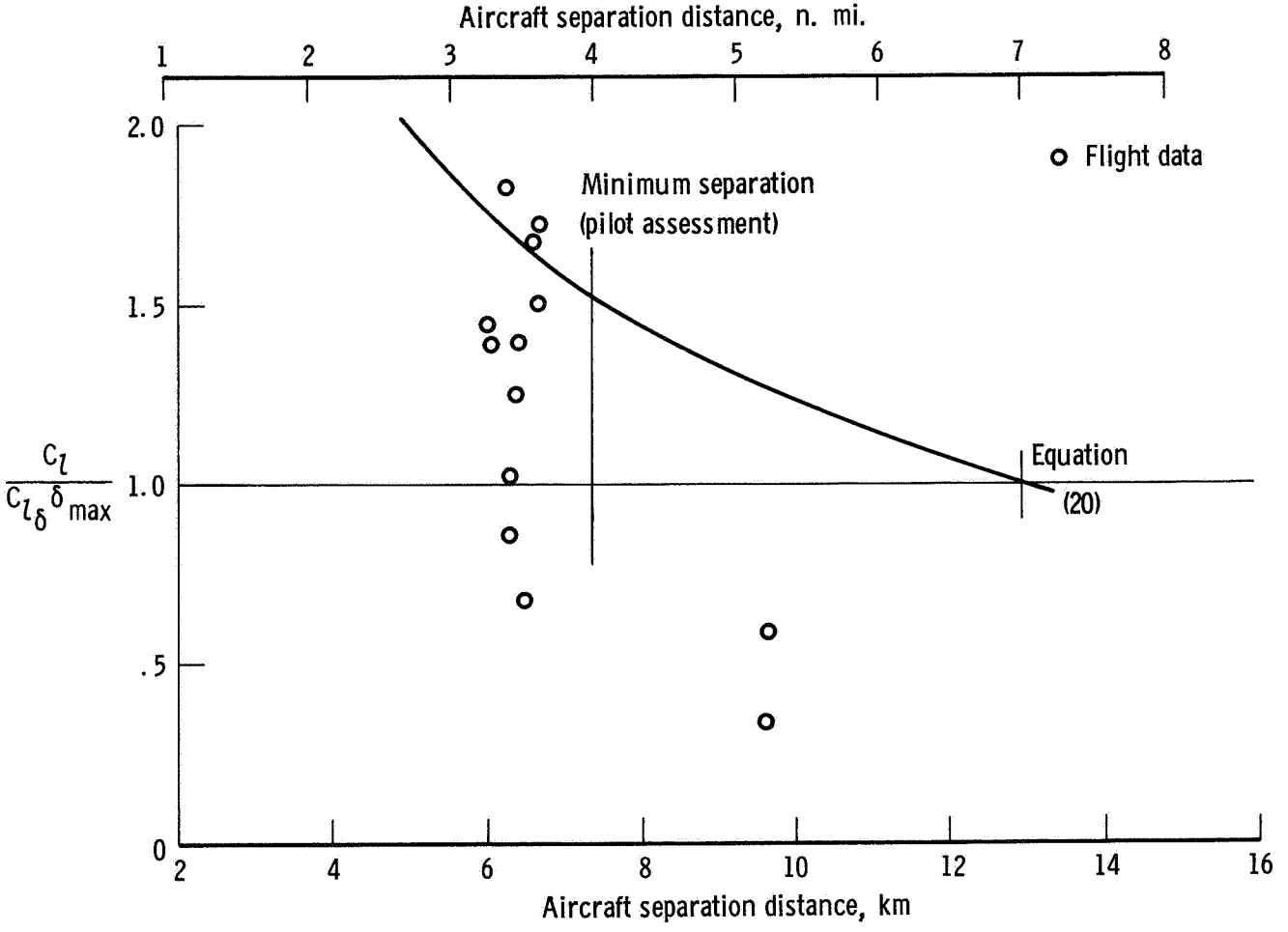

(j) Probe airplane: Learjet 23, landing configuration, V = 181 knots; generating airplane: Convair 990.

Figure 14. Continued.

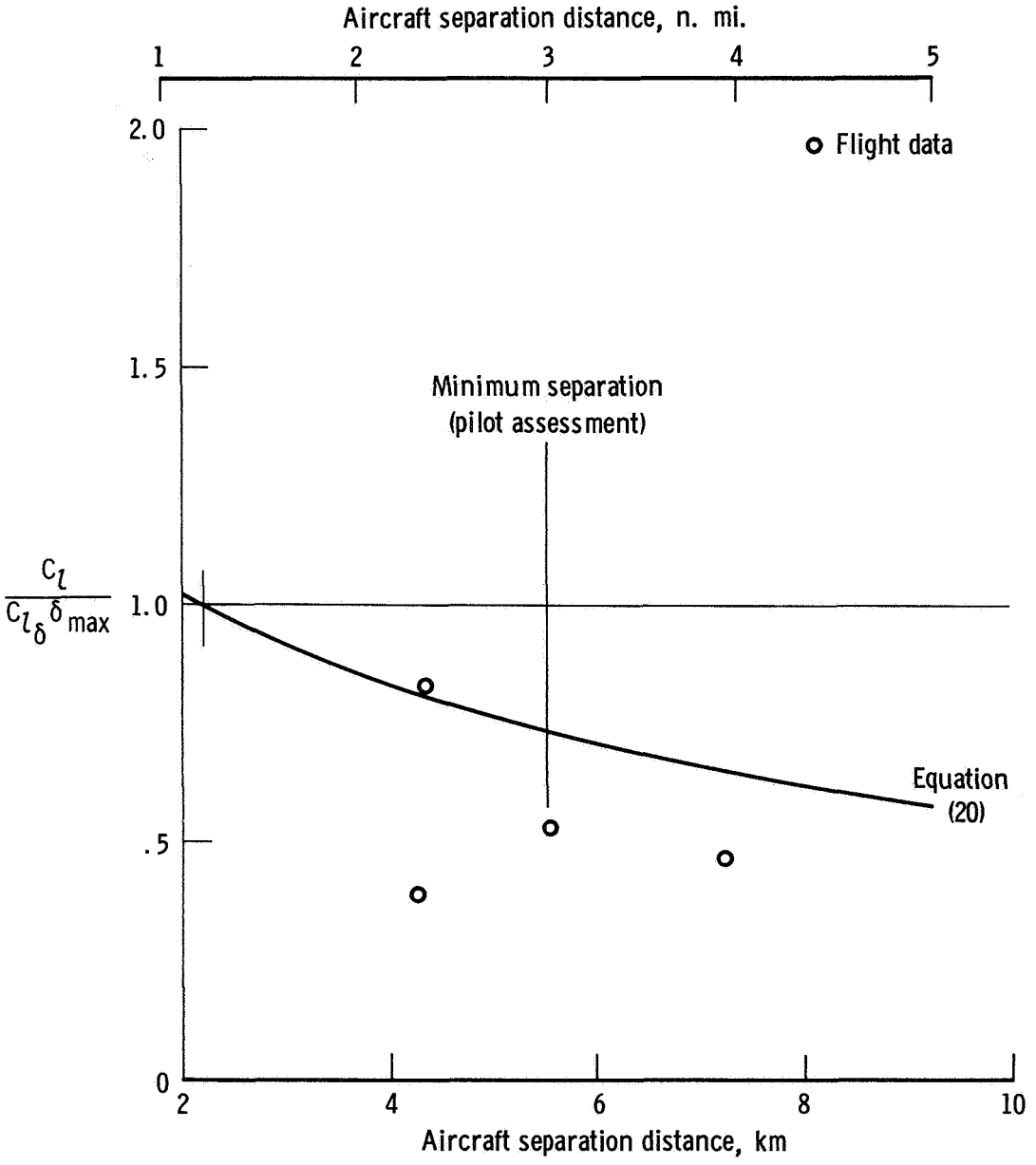

(k) Probe airplane: DC-9, landing configuration, V = 181 knots; generating airplane: Convair 990.

Figure 14. Concluded.

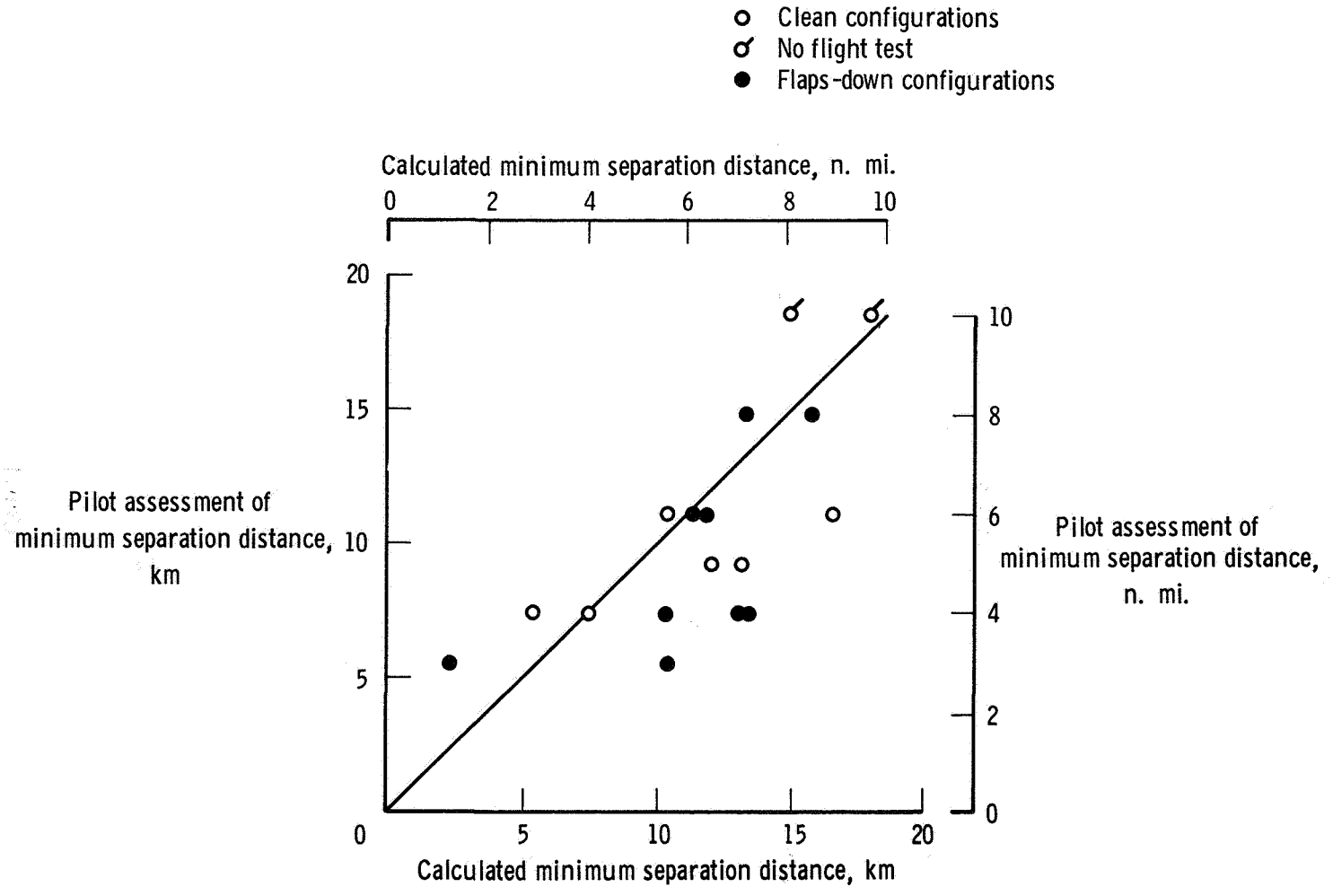

(a) Comparison with pilot assessment.

Figure 15. Evaluation of the minimum separation distance criterion derived from the interpolated expression (eq. (20)) and maximum lateral control power.

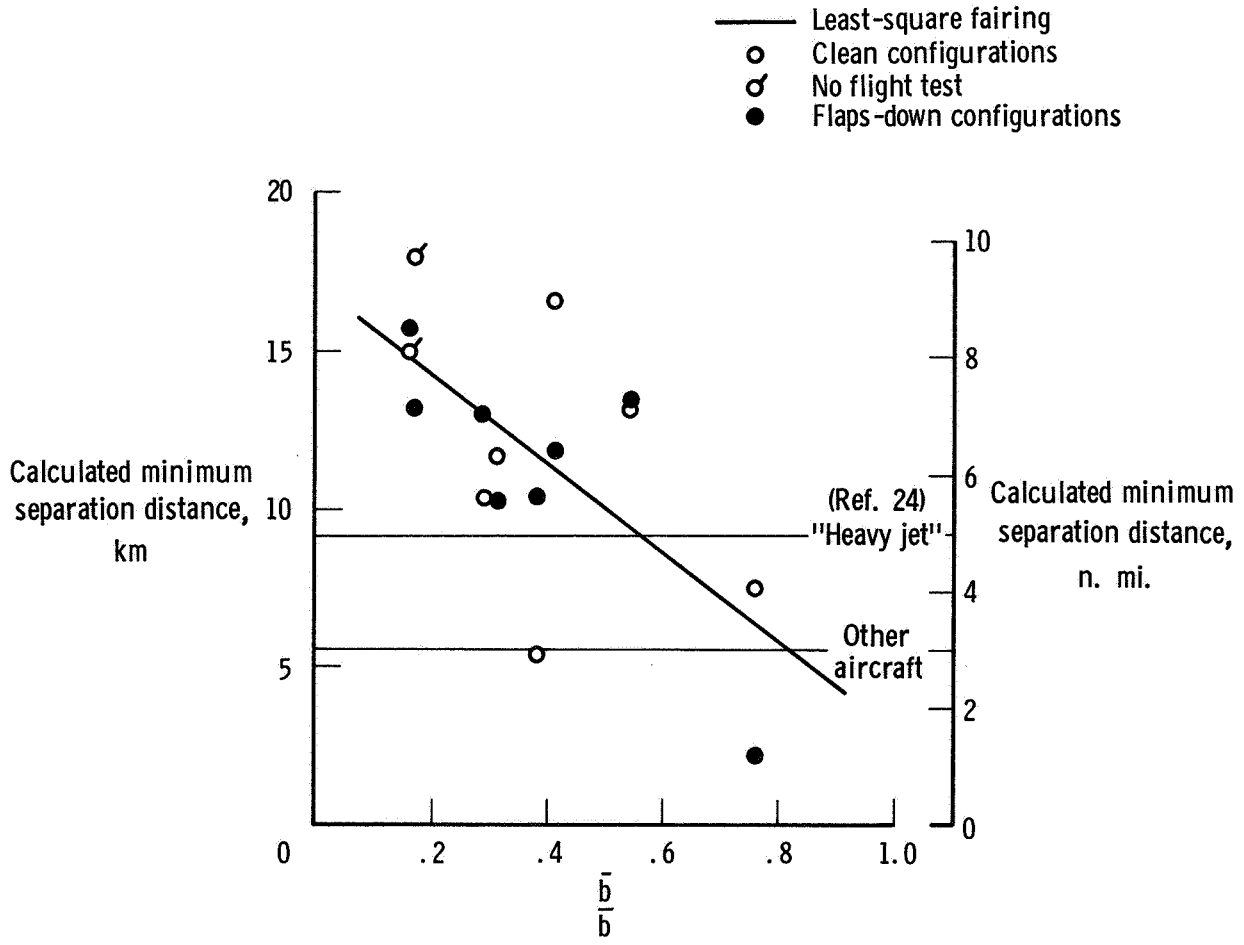

(b) Comparison with probe/generating aircraft wingspan ratio.

Figure 15. Concluded.

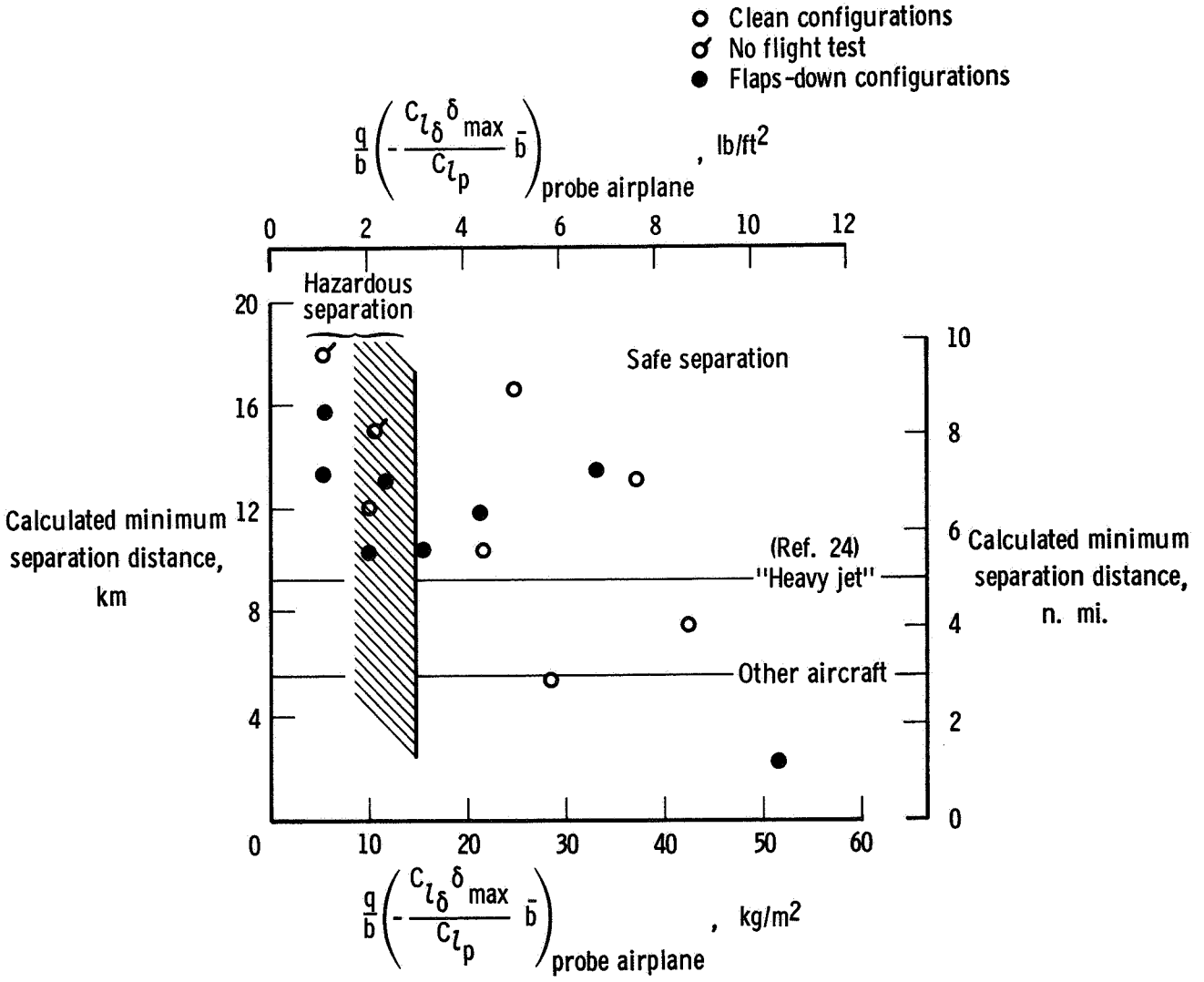

Figure 16. Evaluation of the minimum separation distance criterion (eq. (20)) and the vortex hazard expression (eq. (19)).

NATIONAL AERONAUTICS AND SPACE ADMINISTRATION
WASHINGTON, D.C. 20546

OFFICIAL BUSINESS
PENALTY FOR PRIVATE USE $300

SPECIAL FOURTH-CLASS RATE BOOK

POSTAGE AND FEES PAID
NATIONAL AERONAUTICS AND SPACE ADMINISTRATION
451

U.S.MAIL

POSTMASTER: If Undeliverable (Section 158 Postal Manual) Do Not Return

"The aeronautical and space activities of the United States shall be conducted so as to contribute . . . to the expansion of human knowledge of phenomena in the atmosphere and space. The Administration shall provide for the widest practicable and appropriate dissemination of information concerning its activities and the results thereof."

—NATIONAL AERONAUTICS AND SPACE ACT OF 1958

NASA SCIENTIFIC AND TECHNICAL PUBLICATIONS

TECHNICAL REPORTS: Scientific and technical information considered important, complete, and a lasting contribution to existing knowledge.

TECHNICAL NOTES: Information less broad in scope but nevertheless of importance as a contribution to existing knowledge.

TECHNICAL MEMORANDUMS: Information receiving limited distribution because of preliminary data, security classification, or other reasons. Also includes conference proceedings with either limited or unlimited distribution.

CONTRACTOR REPORTS: Scientific and technical information generated under a NASA contract or grant and considered an important contribution to existing knowledge.

TECHNICAL TRANSLATIONS: Information published in a foreign language considered to merit NASA distribution in English.

SPECIAL PUBLICATIONS: Information derived from or of value to NASA activities. Publications include final reports of major projects, monographs, data compilations, handbooks, sourcebooks, and special bibliographies.

TECHNOLOGY UTILIZATION PUBLICATIONS: Information on technology used by NASA that may be of particular interest in commercial and other non-aerospace applications. Publications include Tech Briefs, Technology Utilization Reports and Technology Surveys.

Details on the availability of these publications may be obtained from:

SCIENTIFIC AND TECHNICAL INFORMATION OFFICE

NATIONAL AERONAUTICS AND SPACE ADMINISTRATION

Washington, D.C. 20546